INVESTIGATIONS AND SUBSEQUENT ADVANCEMENT OF A HOLOGRAPHIC INTERFEROMETRY SYSTEM

Thesis

Submitted to

Graduate Engineering & Research

School of Engineering

UNIVERSITY OF DAYTON

In Partial Fulfillment of the Requirements for

The Degree

Master of Science in Aerospace Engineering

by

Patrick Clayton Wade

Wright Laboratory

WL/FIMO

Wright-Patterson AFB, OH 45433-7005

May 1997

INVESTIGATIONS AND SUBSEQUENT ADVANCEMENT OF A HOLOGRAPHIC INTERFEROMETRY SYSTEM

APPROVED BY

Franklin Eastep, Ph.D.
Advisory Committee Chairman
Professor, Mechanical and
Aerospace Engineering Department

George Seibert, Ph.D.
Committee Member
Supervisor, Experimental Diagnostics
Wright Laboratory

Louis Boehman, Ph.D.
Committee Member
Professor, Mechanical and
Aerospace Engineering Department

Donald L. Moon, Ph.D.
Associate Dean
Graduate Engineering Programs & Research
School of Engineering

Joseph Lestingi, D. Eng., P.E.
Dean, School of Engineering

ABSRACT

INVESTIGATIONS AND SUBSEQUENT ADVANCEMENT OF A HOLOGRAPHIC INTERFEROMETRY SYSTEM

Name: Wade, Patrick C.
University of Dayton, 1997

Advisor: Dr. Franklin Eastep

Non-intrusive measurement techniques for various flow parameters are important in the future of ground testing. The most promising such technique for hypersonic wind tunnels with low densities is Holographic Interferometry. Several improvements were made to an existing Holographic Interferometry system in an effort to advance the technique.

An existing single plate Holographic Interferometry system was modified for use in the laboratory environment. Holograms created in a previous wind tunnel test were examined to validate the use of Phase-shift Interferometry to remove any effects due to any illumination disparities. Using this phase map, a qualitative view of a flow was created. During the reconstruction of the holograms, difficulties with the alignment of the two reference beams were discovered with the single plate method.

In an effort to reduce these errors, the single plate system was modified to a dual plate system, reducing the alignment problems. This dual plate system was used in a laboratory setting to validate the new system. The reader system was modified to perform Phase-Shift Interferometry for the dual pate system. System validation was performed on

a candle, heat gun, and a blowing jet. A phase map for each of these items was created using this modified system.

A user-friendly Windows-based data reduction program was developed to provide qualitative results for all of the images taken. Two computer algorithms were developed to remove the 2π ambiguities resulting from the finite fringes. These algorithms, spiral method and the largest neighbor method, were both developed in an attempt to provide noise insensitive unwrapping of the images. Both of these methods are explained and compared. Once the 2π ambiguities have been removed, the linearly changing reference fringes are subtracted off and the final phase maps are created.

From these unwrapped phase maps, a computer code was developed to calculate the density. The density calculations were attempted on two-dimensional and axisymmetric flows. The flows examined were taken from a 10 degree half-angle wedge at Mach 3, an 8 degree half-angle sharp-nose cone at Mach 6, and a blowing jet taken in the laboratory.

ACKNOWLEDGEMENTS

The author wishes to express his sincere gratitude to the many individuals whose support made this research possible. In particular, thanks are due to the author's supervisor, Dr. George Seibert, for his continuous encouragement and support during the course of this work. Special thanks are due to Linda Smith for providing the background required for this project and for the tunnel test data without which this project would not have been possible. Also, thanks are due to Dr. Charles Tyler for his support in the lab and many helpful suggestions along with the members of the Experimental Diagnostics Research section: Glenn Williams, Hank Baust, and Tom Buetner for their support. Appreciation is also expressed to the faculty advisor Dr. Franklin Eastep for his support. The author appreciates the efforts of the wind tunnel facility crew. Thanks also to the United States Air Force for the resources necessary to conduct this project.

TABLE OF CONTENTS

LIST OF ILLUSTRATIONS

LIST OF SYMBOLS

Symbol			Units
I	=	intensity of light at a given point	----
I_o	=	maximum intensity	----
K	=	Gladstone-Dale constant	m^3/kg
L	=	length of the model being integrated across	m
M	=	freestream Mach number	----
N	=	wave number	----
n	=	index of refraction	----
n_o	=	known index of refraction	----
P	=	static pressure	kPa
P_o	=	stagnation pressure	kPa
r	=	radius from model centerline	m
α_s	=	recorded scene beam angle	degrees
α_s'	=	reconstruction angle	degrees
Φ	=	optical pathlength	m
ϕ	=	phase of light	----
λ	=	recording wavelength	m
λ'	=	recording wavelength	m
θ_c	=	angle of reconstruction reference beam	degrees
θ_r	=	angle of recording reference beam	degrees

ρ	= static density	kg/m^3
ρ_o	= stagnation density	kg/m^3
ρ_∞	= freestream static density	kg/m^3

CHAPTER I

INTRODUCTION

The hypersonic flight regime has become an increasingly important regime in research due to the increased speeds of flight vehicles and missiles. Hypersonic aerodynamics has been a neglected field because of the difficulty of making measurements and the lack of practicality. There is a great need for flow data in this regime to provide data required for vehicle development and computational fluid dynamics code validation.

The traditional method to collect flow data in wind tunnels is by utilizing Pitot probes and hot wire probes. The disadvantage of these techniques is that the probes disturb the flow being measured. In order to overcome these disadvantages, non-intrusive techniques have been developed using optical methods. Some common non-intrusive techniques include Laser Velocimetry,[1] Laser-Induced Fluorescence,[2] Rayleigh scattering,[3] and Doppler Global Velocimetry.[4]

Hypersonic flight research has been focused on flights of altitudes on the order of 100,000 feet or higher where the pressure, temperature, and density of air are substantially reduced. The hypersonic research tunnels located at Wright Patterson are designed for these conditions. With densities around 0.03 kg/m^3 and temperatures around 60-70 K, measurements in the Mach 6 High Reynolds Number Facility (*HRNF*) Wind Tunnel become difficult.

The combination of the low pressures and temperatures along with very high speeds presents excessive challenges for the non-intrusive techniques. The techniques that require the seeding of the tunnel such as Laser Velocimetry or Doppler Global Velocimetry become inaccurate in the high speed realms.[5] The seed particle is unable to follow the flow at hypersonic flow speeds, thus providing erroneous data. The current laser power in specific wavelengths and the very low densities present in the facilities prevents Laser-Induced Fluorescence from achieving its potential for providing flowfield data. Rayleigh scattering was researched extensively for use in Wright Patterson's facilities, however this technique is highly susceptible to errors caused by the condensation of carbon dioxide occurring at the low temperatures encountered in the freestream.

The most effective measurement techniques for use in the hypersonic facilities are based on the diffraction of light through a density gradient. The three most common methods using this principle are shadowgraph, schlieren, and interferometry; all of which consist of propagating a collimated beam through the disturbed area being examined.[6]

Shadowgraph is the simplest of the light diffraction methods. The collimated light is bent due to the changes of index of refraction in the test section and then illuminates a screen. The index of refraction changes can be observed as light and dark lines which correspond to the second derivative of the density. Although shadowgraph

is the simplest to use, however, it is most useful only where large, abrupt changes in index of refraction exist.

The Schlieren method is a very common technique for visualizing supersonic and hypersonic flows. This method varies from the shadowgraph in that after the beam passes through the test section, the light is then focused down to a point where a knife edge is used to clip the bottom half of the light. The image is then displayed on a screen. This method gives the gradient of the index of refraction, i.e. the first derivative of the density.

Interferometry is the most accurate of the three methods but is also the most difficult to set-up. An interferometric system displays the density as a fringe pattern which is created by the interference of two coherent waves. The two waves used to create the interference must travel separate paths, and the differences in the two paths is displayed as this fringe pattern.. The optical difficulty in set-up arises from the fact that the pathlengths between the two separate paths must travel indentical distances. The benefit of interferometry is that unlike the shadowgraph and schlieren methods, this techniques provides a direct measurement of density rather than one of the derivatives.

In holographic interferometry (HI), the use of a hologram allows the two waves to be displaced temporally rather than spatially as is common in most interferometry systems. Using temporally separated waves eliminates the most difficult problem in interferometry since the two waves travel the exact same path, the distances traveled

between the two are identical. However, interference is only created when the two waves arrive at the detector simultaneously. This is accomplished using a recording of the beam that permits its exact reproduction at later times. It should be noted that the signal and recording beam pathlength differences must be within the coherence length of the laser.

Holography allows the complete reproduction of a wave, rather than just the intensity. The complete reproduction of a wave includes its phase information which is lost in standard photography. Using two holograms taken with the same system optics but at different times allows the analysis of the change in index of refraction over the same point in space at the two different times. The two holograms are taken such that the first one corresponds to the flowfield undisturbed and the second one corresponds to the disturbance. The quality of the optics is not as critical for *HI* as it is for the other two light diffraction methods. Optic irregularities are eliminated in the interferogram since only the differences between the two shots are displayed in the interferogram.

There are three main types of holograms, only two of which are useful for flow diagnostics. The three types are reflection holograms, diffuse holograms, and direct holograms. Only the latter two are useful in flowfields since the former method relies on the reflection of the signal beam from the target. The reflection hologram is the common type used for holographic artwork because it produces a clear three-dimensional image of the target.

The diffuse hologram method creates an image backlit by a plane of light passing through the diffuser. The diffuser and the collection optics are located on opposite sides of the tunnel, allowing the diffuse laser light to pass through the test section. The main benefit of this method derives from the fact that the light scattered by all points on the diffuser passes through all parts of the test section allowing the object to be examined at different angles. This method was rejected for use in this project for two main reasons. The diffuser greatly reduces the amount of light that is able to be collected because the light is scattered when it passes through the diffuser. Secondly, there is a large increase in laser speckle produced in this method. This noise greatly complicates the unwrapping process which will be discussed later.

The type of hologram created by directly passing the collimated beam through the test section is known as a direct hologram.[6] Since the area of interest is located in the portion where the light is collimated, the interpretation of the fringes is simplified. This method also produces far less speckle than the diffuse method. The drawbacks are that the image of the object is seen backlit by a point of light due to the collimation. Also, since each ray of light exposing the photographic plate corresponds to a specific ray that passes through the test section, the plane of interest can only be examined for the specific angle that the hologram was recorded with.

Holographic interferometry can be separated into two categories: single plate, dual-shot interferometry and dual plate, single-shot interferometry. The single plate method overlays the two holograms on one plate using different reference angles to

reproduce the holograms individually. With the dual plate method, the undisturbed and disturbed flow holograms are taken on separate plates. The plates are then sandwiched together, reproducing both plates simultaneously, creating the interference patterns.

The Wright Laboratory Flight Dynamics Experimental Diagnostics branch received a holographic interferometry system under a Small Business Innovative Research contract with KMS Fusion, Inc. Under this contract, a single plate *HI* system for use in the hypersonic facilities was designed and a play-back system was provided to allow phase shifted interferograms to be captured using a CCD camera. Smith reconfigured the design to allow for implementation into the facilities and operated the system in the Mach 3 wind tunnel to examine the flow around a wedge in an effort to provide validation of the system.[7] The entire hologram recording portion of the system was later modified for use in the Mach 6 *HRNF* where investigations of rope wave propagation were examined on a sharp nose cone.

Qualitative results from *HI* systems have been around for many years as was the theory of converting *HI* to a quantitative technique. However, this was not common due to the lack of computing power required. The power and speed of modern computers allow this feat to finally be accomplished. A data reduction program was developed using the principles established by Vest[8] in an attempt to convert the qualitative data provided from the Mach 6 tunnel tests to quantitative results. After problems were encountered while attempting to analyze the data, the HI recording

system was reassembled in a laboratory setting in an attempt to acquire data in a better controlled environment.

It was discovered that the problems, encountered while attempting to analyze the Mach 6 data, were inherent to the single plate method due to the use of different laser wavelengths for the recording and playback of the holograms. In order to overcome this inherent source of errors, the system was modified to allow the use of the dual plate method. The dual plate *HI* system uses holograms that are recorded on two separate plates using a special dual plate holder rather than the dual holograms on a single plate as is used in the single plate method. The advantage of this method is that the recording angle is kept constant, so only one beam is required for the play-back system, simplifying the play-back system tremendously. The drawback, however, is that since there is only one beam, the phase shifting must be performed through rotation of the plates rather than altering one of the play-back beams.

A computer code developed for the conversion of the qualitative data into quantitative data was produced using the traditional theory as presented by Vest.[8] This code was designed to operate on a PC compatible computer and was created in Visual Basic to allow for a user-friendly environment. The most difficult portion of any quantitative *HI* code is the removal of the 2π ambiguities created when the phase of the fringes is established. An attempt to fully automate this process further complicated this task. Using an innovative algorithm, the ambiguities were removed more accurately than had been done in previous real images. Due to the noise observed on

the tunnel test data, this algorithm was specifically designed to be less susceptible to noise than previous techniques. Once the phase has been unwrapped, the density can be calculated. Limited by the use of direct holography and only one view, the density can only be accurately calculated for two-dimensional or axisymmetric cases.

One purpose of this report is to present the advantages and disadvantages of the single plate dual-shot and dual plate dual-shot HI systems. The primary goal of this research was to create the computer code capable of converting qualitative interferographic data into quantitative density data. The various algorithms developed for the computer code will be discussed in detail. Limited results of a candle flame, heat gun, blowing jet, and Mach 6 cone tests will be presented.

CHAPTER II

SINGLE PLATE HOLOGRAPHIC INTERFEROMETRY

A single plate, dual-shot holographic interferometry system was utilized at Wright Laboratory in two facilities. The principle of this system is to reproduce two waves passing through a medium using only one photographic plate. By using a different reference angle to create the two holograms, the two holograms can be created independently and through the use of the reader system setup can be phase shifted with respect to one another rather easily.

EXPERIMENTAL SETUP

Hologram Recording System

The Mach 6 *HRNF*, High Reynolds Number Facility, single plate, dual shot holographic interferometry system is shown in Figure 1. The illumination source for this system is a Class IV ruby laser, which has a wavelength of 694nm. The main advantages of this laser are the tremendous pulse power of 3 joules and the pulse length of 15 nanoseconds. This combination of power and very short pulse duration allows the flow to be "frozen" such that instabilities can be analyzed without the phenomenon being integrated with time.

Attached to the rear of the ruby laser is a small Helium-Neon laser rated in the 18mW range. This laser is aligned with the ruby laser path allowing low powered

continuous laser light to be used to align the system without the risk of damaging any optics. This He-Ne laser was also used in a system modification designed to allow for the qualitative, real-time viewing of flow phenomena at Wright Labs wind tunnel facilities.

The laser beam is turned by a high-energy reflective mirror to pass down the table towards the remainder of the optics, then it is split creating the signal and reference legs of the system. By using this method to create the two legs of the system, the beams are kept coherent with respect to each other, a requirement for the creation of a hologram. The signal beam is then passed though a microscope objective to expand the beam into the concave mirrors. The focus of the microscope objective is set at the focus of the mirror to produce a collimated beam across the flowfield of interest. After the beam passes through the test section, the beam is then focused down using a duplicate concave mirror. The beam is then directed into the holographic plate holder for recording. The size of the illumination spot is about 2 inches in diameter on the holographic plate. The angle of the plate holder to the main axis of the concave mirror is opposite of the angle on the recording table in an effort to reduce any errors produced by the use of concave mirrors off-axis.

After being split, the reference beam is sent to a tower where it is turned down to allow passage under the wind tunnel. The beam is then turned back up to the height of the optics on the recieving table. A microscope objective and collimating assembly are used to produce a collimated beam 2 inches in diameter that is required to complete

the hologram. Two different reference angles are created using a removable, plane mirror which is removed between shots. Plane mirrors pass the parallel light to the holographic plate where it interferes with the signal beam passed through the test section. This completes the hologram and permits the signal beam to be reproduced using the reference beam.

Reader System Setup

The reader system is shown in Figure 2. The laser used in this system is a laser diode with a wavelength of 672nm and a power of 10mW. As shown, the output of the laser is split by a 50/50 beam splitter cube into each of the legs required for the playback of the two holograms. Each beam is then split by a piece of glass inserted into the beam paths. The main portion of the beam is sent through the glass where it passes through a microscope objective. This optic focuses the beam to a point where it passes through a spacial filter in an attempt to refine the beam uniformity. The point of light then expands until it is about 2 inches in diameter. At this point, the beam passes through a lens located such that the focal point of the lens is at the spacial filter. This setup produces a collimated beam which is used to reproduce the signal plane wave when the beam illuminates the hologram at the same angle that the hologram was recorded. The light reconstructed through the hologram is reflected through a mirror and is finally imaged on a CCD camera with a 150mm zoom lens. This lens allows the region of interest to be enlarged so that it can be analyzed.

As previously mentioned, each leg of the reader system is split by a piece of glass inserted into the beam paths. Both of the reflections from the glass are passed through a recombining optic designed to superimpose the two beams. Because these beams are coherent and colinear with each other, they form an interference pattern all along the beam paths. The beams are then passed through a microscope objective in order to expand this interference pattern. The expanded wave is then passed through a cylindrical lens to elongate the interference pattern such that it can be monitored through the use of a photodiode detector. Using the readout from this detector, the phase shift of the beams with respect to one another can be monitored, and this directly correlates to the phase shift imaged by the CCD camera.

The mirror used to turn one of the legs of the reader system is placed on a piezoelectric motor which is used to drive the mirror fractions of a wavelength in distance. Slightly translating the mirror causes the pathlength of that leg of the reader system to alter slightly. This change manifests itself in a shifting fringe pattern on the imaging system.

RESULTS

Prior to a detailed analysis of the holographic plates taken from other wind tunnel tests, the single plate holographic interferometry system appeared to be the best system for the facilities located at Wright Laboratory. The single plate holographic system has many advantages to the dual plate system. These advantages include the

need for only one plate to be used per shot and the ease of use in the facilities because only one mirror must be removed between shots. The main advantage of this system is the ease of phase shifting the interferograms in the reader system.

Interferometry data provides a phase map which contains only the phase of the light without any background noise such as ambient light or optical aberrations. This phase map allows a qualitative analysis to be made directly from the phase map itself, and the density to be calculated through the use of software. The fundamental equations[9] that allow the decoupling of the phase from any other light sources are

$$I_1 = I_o(x,y)\left[1+\gamma\cos\left(\phi+\frac{\pi}{4}\right)\right] \tag{2.1}$$

$$I_2 = I_o(x,y)\left[1+\gamma\cos\left(\phi+\frac{3\pi}{4}\right)\right] \tag{2.2}$$

$$I_3 = I_o(x,y)\left[1+\gamma\cos\left(\phi+\frac{5\pi}{4}\right)\right] \tag{2.3}$$

From these three independent equations, the three constants, I_o, γ, and ϕ can all be calculated. For interferometry, only the phase of the images is required to determine the index of refraction gradient. Using the three image method, ϕ can be calculated as

$$\phi(x,y) = \tan^{-1}\left[\frac{I_3(x,y)-I_2(x,y)}{I_1(x,y)-I_2(x,y)}\right] \tag{2.4}$$

Once the phase has been eliminated from the other noise, a qualitative view of the flow can be displayed without any interferences from background light or other

sources of errors. As will be discussed later, the curvature of the fringes in this image corresponds directly to the change in index of refraction.

The single plate hologram recording system was used twice in the wind tunnels at Wright Laboratory. The first time it was used was to study a two dimensional flow over a 10° wedge at speeds of Mach 3. This test was performed by Smith[7] and presented as a proof of technique, but the data was never phase shifted due to the lack of a data reduction software package. Figure 3 shows an example of one of the images digitized from this tunnel test. When combined with two other images which have been shifted according to Equations 2.2 and 2.3, a phase map can be calculated which eliminates many of the errors in the image. A phase map is shown in Figure 4 clearly displaying the shock wave off of the sharp point of the wedge and the boundary layer along the surface of the wedge. The waves passing through the freestream are turned as they enter the shock wave and have a different shape displaying the change in the index of refraction and thus density.

The poor quality of the phase map is due to the poor quality of the hologram. The photographic development process of the holograms recorded during this tunnel entry was varied in an attempt to optimize the hologram quality. Unfortunately, very few of the holograms are of a quality necessary to obtain useful data. This tunnel test was performed only as a proof of concept and an attempt to optimize the holography system .

After the HI system was tested in the Mach 3 facility, it was utilized as a primary diagnostic in an attempt to research hypersonic rope-wave development over an 8° half-angle, sharp-nose cone in the Mach 6 wind tunnel. It was believed that the short pulse duration of the ruby laser would provide an instantaneous "snapshot" of the flow, thereby capturing the rope-wave structure for post-analysis. The wind tunnel stagnation pressures were varied through the range of 300-1000 psi in an attempt to produce various rope-wave structures.

It was believed prior to entry into the wind tunnel that the extreme drag force exerted on the model and the sting at test conditions would shift the model between the reference and signal shots. In order to analyze the images accurately very close to the model surface, knowledge of the model location had to be known to the order of a pixel. A shift of a few pixels in model location between the two shots would make it impossible to know the location to the required accuracy. As a means of overcoming this problem, the reference shot was taken with the model out of the field of view. Unfortunately, this action led to other problems which will be discussed later.

During the test, over 200 dual-shot, single plate holograms recording instantaneous views of the flowfields were produced. After the test was completed, the plates were analyzed to acquire flow data. Figure 5 shows a representative interferogram of the data collected. The visibility of the shockwave in the image can be amplified through the use of a phase map from the phase shifted images. Once again using Equation 2.4 to calculate the phase map, the flow structure is clearly shown through-

out the entire flowfield as seen in Figure 6. A qualitative view of the flowfield can be shown with minimal computer time required. Thus, as a qualitative tool, HI provides an excellent view of the flow. The benefits of using holograms instead of just photographs is that a hologram can be later recreated in the laboratory environment. Additionally, due to the properties of a hologram, a small portion of the flowfield of interest can easily be expanded and viewed at various levels.

ERRORS

As the data from the wind tunnels was analyzed, many sources of error were identified that prevented an accurate quantitative analysis of the flowfields. However, since the computer program utilized in the analysis was not complete until after the tunnel test, the errors were not able to be corrected during the test. The major errors encountered in the Mach 6 *HRNF* tunnel entry were due to the set-up, the development of the holographic plates and the use of different wavelength lasers to record and playback the holograms. These errors caused, at best, poor quality holograms to be created.

These causes of the poor hologram creation were determined after the tunnel entry had concluded and have since been corrected in the current set-up. The primary problem during the test entry was the ratio of the signal to reference beam intensities which was about 1:1. The correct settings should be within the range of 1:2 to 1:10.[10]

The current set-up uses a signal to reference beam intensity ratio of 1:5, within the optimum ranges.

Polarity matching between the signal and reference beams is also critical for hologram quality. A slight misalignment of the ruby laser cavity causes the beam to contain multiple polarities and thus produces interference patterns. This interferes with the production of the hologram since only coherent beams are able to interfere and produce the hologram. The solution to this problem without major laser realignment was to position a polarization filter directly in front of the holographic plate. This allows only one polarization to pass through and eliminates the unwanted interference patterns located mainly in the signal beam.

The largest cause of the poor or nonexistent holograms was the photographic developing. The chemicals used to develop the plates taken during the tunnel entry were of the wrong concentrations and the time the plate was exposed to each chemical bath was incorrect. This created a holographic plate that contained a poorly developed image that was unable to properly reproduce the signal beam.

Even though the above mentioned errors caused large amounts of noise in the image complicating the unwrapping, they did not change the phase map values. For the qualitative data, the primary source of this error was the use of a reconstruction laser which has a different wavelength than the recording source. This change in wavelength is not an inherent problem, but aligning the two holograms using the current setup becomes a major problem. The angles of a hologram reconstruction are

a function of the recording reference beam and signal beam angles, the angle of the reconstruction beam, and the two different wavelengths of the lasers used. Lanen[11] shows this equation to be

$$\alpha_s^{'} = \sin^{-1}\left[\frac{\lambda^{'}}{\lambda}(\sin\alpha_s - \sin\theta_r) + \sin\theta_c\right] \tag{2.5}$$

where $\alpha_s^{'}$ is the reconstruction angle, λ and $\lambda^{'}$ are the recording and playback wavelengths respectively, α_s is the recorded scene beam angle, and θ_r and θ_c are the reference angles during recording and playback. All angles in this equation are measured normal to the holographic plate.

The tunnel test was designed so that the angles between the reference beams used in the dual-shot single plate hologram recordings were identical to the angles of the two beams in the reader system, 9.5°. If a laser of the same wavelength was used in both the recording and playback of the hologram, the two images obviously would be superimposed. However, with the recording wavelength of 694nm and the playback of 670nm, this is not the case. For identical recording and playback reference beam angle differences, the reconstructed images are offset by 0.332°. Even this small shift, with an otherwise perfect alignment, forces the plate to be pivoted 11° from its required position. This leads to small errors in the reconstruction since the hologram is being replayed at a different angle than it was recorded. This becomes even more apparent if the recording angle separation is not equal to that of the reader system. Since the angles of the recording beams were not able to be measured accurately, it

is not unreasonable to assume that errors of a couple of degrees in the separation could exist. Using this small change in Equation 2.5 leads to the plate having to be rotated over 45° in order to align the two holograms. The principal errors caused by this rotation of the holographic plate consisted of wavefront distortions in the reproductions causing curvature in the reference fringes and a marked dimming of the reproduced holograms. The only possible method to eliminate these errors after the plates have been recorded is to alter the angles of the reference beams with respect to each other.

If the single plate method is used in the future, the angle errors can be completely eliminated during the set-up using an alignment hologram. If a dual-shot hologram is created from the reader system, this alignment can be done exactly. Adding a beam splitter before the first optic in the reader system allows the creation of a signal beam to be used as an alignment beam. By blocking one of the reader system beams, a hologram can be recorded using the remaining reader system beam as the reference beam and the new split beam as the signal beam. The hologram is created on the same plate using the previously blocked reader system leg and blocking the leg that was used earlier. The signal beam used in the new hologram is the identical beam that was used in the first imaging. The plate is then developed and placed in the holographic recorder system.

For alignment of the recorder system, the signal beam on the holographic recorder needs to be blocked and the removable mirror must be replaced with a beam splitter.

This allows the two reference legs of the recorder to pass into the holographic plate while blocking out the signal beam passing through the test section. The alignment must be done with the laser that will be used for the recording of the holograms. This becomes difficult to align because the ruby laser used in these tests is pulsed. By placing a piece of burn paper along the path of the reproduced hologram, the errors in alignment appear as spacing between the two simultaneous reproductions. By altering one of the reference legs, the reproductions can be moved closer together until they become colinear, ensuring exact alignment taking into account the differences in wavelengths used.

CHAPTER III

DUAL PLATE HOLOGRAPHIC INTERFEROMETRY

Most of the disadvantages of the single plate, dual-shot interferometry system can be eliminated using the dual plate method. The dual plate HI system was used in the 1970's at Wright Laboratory by Havener.[10] Since computer power to analyze the data collected was unavailable, interferometry was discontinued in the Wright Laboratory facilities for about 10 years until the computers progressed enough to allow the quantitative possibilities of this technique to be realized.

EXPERIMENTAL SETUP

The setup of the dual plate holographic interferometry system is very similar to that of the single plate method. The only differences in the recording system are on the receiving table. The removable mirror is kept in the path of the reference system. Even though the leg without this mirror produces a more rounded beam due to the extra off-angle turn caused by the removable mirror, the second leg allows a lateral match of the beam once the beam is expanded. It is important once the beam is expanded to ensure that any aberrations in the laser beam are aligned to achieve the best possible interference in the hologram creation. The holographic plate holder located at the intersection of the signal beam and the reference beam is replaced by a special dual plate holder instead. This dual plate holder is designed such that the

plates can be slid in and out of the plate holder with ease. For the reference shot, the ruby laser light passing through the undisturbed object plane exposes an unexposed photographic plate. The plate is then removed from the plate holder and is placed in a box until it is developed. A different unexposed plate is then placed in the same slot of the plate holder and the ruby laser is fired again; however, this time the laser light is passed through the disturbed object plane.

The reader system used for the playback of the dual plate holograms is very different than the setup for the single plate system because only one reference beam, rather than two beams, is used to recreate the holograms. This beam, originating from the laser diode, is passed through a microscope objective, a pin hole, and then a lens to create a collimated beam that is used to recreate the hologram. The holographic plates recorded and developed previously are then placed in a dual plate holder in the reader system and the recreated hologram is then viewed using a CCD camera.

The difficulty of the dual plate system comes from the fact that phase shifting the dual plate system is more complex to implement than for the single plate system. For the dual plate system, the only means of shifting the phase is by translating the plates with respect to each other. This is accomplished most simply by placing the dual plate holder on a rotation stage. The difficulty comes from attempting to determine the rotation required to shift the fringes the required amount. The method that appeared to be the only solution was to capture an image, rotate the stage, and then

capture the new image. By examining these two images and knowing the rotation of the plates, the required phase shift could be determined.

It was desired to develop a computer code to automate this phase-shifting. A stepper motor was attached to the rotation stage to allow computer control of the rotation. A major difficulty came from trying to use the computer to determine the translation of the fringes due to rotation. The lack of a frame grabber that could be accessed by Visual Basic caused the software creation to be greatly complicated. A windows macro was developed that could be called by Visual Basic that would operate the frame grabber software. Once that was accomplished, the automated routine was attempted.

The first method attempted was to examine a 3x3 pixel area located within the image at a point defined by the user. Once this point was established, the image was examined only at that point to determine the average pixel value. A 3x3 pixel region was chosen in an attempt to balance noise tolerance and a small enough point that the software could accurately determine the peaks and valleys. The routine then stepped the rotation stage by a known amount and another image was acquired and the same nine pixels were analyzed. By continually stepping and analyzing along with changing the step sizes, the exact number of steps required for a complete shift can be determined. This routine proved too susceptible to noise and another routine was thus developed.

The second routine operates by examining a line that crosses several fringes in the portion of the image where the reference fringes are straight. The line marks the location of four peaks and valleys in the fringe pattern shown as the light and dark lines respectively. Then, the motor steps the rotation stage a preprogrammed amount. The same line is used on the new image and the location of the peaks are recalculated. Using a small enough step size, the new peak location closest to the original peak location can be used to determined the translation of the fringe down to the pixel level. Once this is known, the program uses the original four valleys to determine the separation of the fringes. Using these two facts, the total rotation required to shift the fringe pattern by one fringe can be calculated, assuming a linear relation between the rotation and the fringe shift. This required amount is then divided by 4 and used to shift the fringe pattern. An image is taken; the plates are rotated the calculated amount and then another image is taken. This is continued until a total of three images are taken which satisfy Equations 2.1, 2.2, and 2.3.

Computer hardware/software interaction problems and noisy images caused neither routine to work well. It was finally decided to include the user in the loop and manually determine the number of steps required. This greatly decreased the complexity of the phase stepping and allowed for data collection at far faster rates than were achieved with either of the attempted routines.

BENEFITS OVER SINGLE PLATE METHOD

The dual plate method provides many benefits over the single plate method. These advantages overcome the increased difficulties in the reader system setup and image collection. One of the benefits is the increased stability of the fringes. With the single plate method, the fringe locations are very sensitive because the pathlength difference between the two different beams used is critical. Any vibrations cause the mirrors on the reader system to shift, and this results in unwanted fringe shifting. The single plate system was very sensitive to all forms of acoustical noise. This noise sensitivity was manifested as fringe movement which causes possible errors during the capturing of the phase shifted images. For the dual plate method in which the two plates are illuminated by the same beam, changes in the beam pathlength effect both images and, as such, there is no change in the fringes. This system is very stable even to direct vibrations of the table.

The dual plate method also eliminates the problems of playback at a different angle shown by Equation 2.5. Since both of the plates are recorded at the same angle, the reconstructed images are displaced by the same amount and thus are still superimposed. This eliminates any errors added by rotating the plate as required in the single plate hologram method to superimpose the two images.

The final advantage of this system comes from the possibility of using the same reference plate for multiple signal plates if nothing has changed in the setup. Since only the disturbed flow condition needs to be taken, data may be acquired faster

thereby increasing test productivity. However, care must be taken to ensure that if any optics have changed or any other conditions have altered, the reference plate must be retaken to allow for accurate interferograms.

RESULTS

The dual plate *HI* system has been used extensively in the laboratory in an effort to produce holograms of the quality required to provide quantitative flowfield information, but has not been used yet in a ground-test facility. The system was scheduled for use in support of a test in the Transonic Gasdynamics Facility (*TGF*), however tunnel problems caused the test to be postponed.

After the dual plate system was developed in the laboratory, various tests were run in an attempt to validate the data reduction code. The dual plate method was used to analyze the heat field produced by a small candle, the heat produced by a heat gun and, finally, the flow exiting a jet.

The first test performed in the laboratory was the imaging of a small burning candle. This was chosen because of the simplicity of the setup and the flowfield. The heat in the candle flame and above it is intense enough to be easily seen in an interferogram. Figure 7 shows an example of an image captured from the candle flame. The curvature of the fringes through the heated region is clearly evident and the area where the bouyancy-induced flow becomes turbulent can be seen in the upper portion of the image.

After some difficulty with the phase-shifting program, the three images required for the unwrapping were captured, and a phase map, as seen in Figure 8, was created using Equation 2.4. The density gradient becomes more prevalent when viewing the phase map rather than just the image since the background noise has been eliminated. The regions of extreme temperature gradient in the candle flame are very evident due to the curvature in that region.

The candle provided a validation of the new setup, however the data acquired from the candle burn was unable to be used in a density calculation because the candle contains a three dimensional density distribution without any symmetries. In an attempt to gain some data useful for the data reduction software, a heat gun was used. It was hoped that the heat gun would still produce the very large density gradients evident in the candle, but would provide improved validation of the software because the circular shape of the nozzle could be approximated as axissymmetric.

An example of the images collected from the heat gun are shown in Figure 9. Once again, the temperature gradients are shown very clearly, and the region where the flow turns to turbulence is also clearly seen. Using the phase map software to remove any background noise, Figure 10 shows the phase map with the 2π ambiguities still present.

The final test of the two plate method was the blowing jet. A small nozzle of a $\frac{1}{4}$ inch diameter is used with varying stagnation pressures in an effort to determine the flow structure of the nozzle. This problem is very complex. A clear picture of the

flow constrained by large flow structure changes in a very small area was very difficult to achieve. An example of a typical image collected is shown in Figure 11. It was hoped to compare the flow out of the jet for various back pressures, so holograms were taken for back pressures of 273.7 and 446.1 kPa. Phase maps were created for both cases using the data reduction software. The representative phase maps are shown in figures 12 and 13 for the 273.7 and 446.1 kPa cases, respectively. Differences can be seen between the phase maps, and as expected the latter case shows the largest density changes. An attempt to convert these phase maps into actual density readings using the data reduction software was made.

CHAPTER IV

DATA REDUCTION SOFTWARE

In an effort to enhance the Holographic Interferometry beyond any capabilities available at Wright Laboratory, a data reduction program was developed. It was hoped that this software would provide the density field for a given two-dimensional or axis-symmetric flow and would later provide the basis of software for future improvements.

In an effort to produce a user friendly system, the code was written in Visual Basic and designed to be run on a personal computer. This will allow the system to be easily used by any trained personnel and the system will hopefully be transitioned to other Air Force units operating the same *HI* system.

The first step of the program is to load the phase shifted images into the computer memory as three arrays established for this purpose. After the images have been loaded, the user is then given the option of cropping the image. This feature allows the user to draw a box of any size around any portion of the image and use only that region in the data reduction. This eliminates borders of the reproduced interferogram and allows for quicker analysis due to the smaller region.

After the region has been cropped, the images are usually filtered to eliminate some noise in the image. This step is not required, but it greatly decreases compu-

tational time in future steps. If the filtering option is chosen, a simple 3x3 median filter is used. The pixel value is defined as

$$\phi_{i,j} = \frac{\phi_{i-1,j-1} + \phi_{i-1,j} + \phi_{i-1,j+1} + \phi_{i,j-1} + \phi_{i,j} + \phi_{i,j+1} + \phi_{i+1,j-1} + \phi_{i+1,j} + \phi_{i+1,j+1}}{9} \tag{4.1}$$

with alterations in the algorithm made for border pixels.

The next step in the data reduction program is to begin the data reduction process. The user is given two options from the menu, to either perform the complete analysis or only calculate the phase map. The phase map only option takes the three images and converts the data into a phase map through the use of Equation 2.4. After this has been completed, the user has the option of displaying the phase map or saving the phase map to a file. If the phase map save option is chosen, the user is given two further options, to either store the image as an *.IMG* file or as a *.GHI* file. The *.IMG* option is designed to allow the image to be compatible to the frame grabber software, Global Lab, so that the image can be displayed and manipulated by this software. The Global Lab software package also allows the image to be converted to *.PCX* or *.TIF* formats, allowing the images to be imported into any image processing packages. The *.GHI* selection is specific to the data reduction software developed for the *HI* system, but it allows the data to be stored as a real value, thus preserving the entire phase map data. The binary storage of *.IMG* files required the real data to be converted to integer values between 0 and 255. A phase map stored in the *.IMG* format is unable to be used for any data reduction.

If the user chooses to perform a complete analysis, the first of the three loaded interferograms is displayed on the screen along with different options to allow for flexibility. The user can set the pixel to length dimensions in either metric or English units. This dimensioning is critical for the axisymmetric cases, and gives the user a sense of perspective when viewing the phase map and density in the display routines. Another option at this screen is for the user to enter the centerline for any axisymmetric models.

If the user desires to further crop an image, this can be done from this screen. The user first draws a line on the image to be used as the border of the cropping, and then clicks on the side of the line to be discarded. This feature allows cropping at non-orthogonal lines, unlike the earlier crop option, and also allows portions of the image to be kept in the original image, that provide useful dimension data or the centerline, without performing an unwrap on these images. The final options on this screen provide the user with various unwrap options which will be discussed in detail later.

Once all of the options have been selected, the user clicks on the completed button and is then prompted to draw a box around the reference fringes located in the freestream. This box allows the calculation of the linear phase change in the unwrapped image caused by these fringes. This change is later subtracted, removing any effects of the reference fringes. The program now uses Equation 2.4 to determine the phase map and afterwards initiate the unwrap routine.

PHASE UNWRAPPING

The most difficult process in quantifying data from a phase map is the unwrapping of the phase. Due to the nature of the inverse tangent used in Equation 2.4, the phase information in the phase map contains 2π ambiguities that must be eliminated for the exact phase shift to be known. The elimination of these 2π ambiguities is a process known as unwrapping of the phase.

This process is straight forward for the one dimensional case without any noisy pixels. A starting point is chosen with the phase shift defined as 0. The routine steps from this starting pixel to the pixels touching it. If the difference between the two pixels is less than π, then the second pixel is said to be unwrapped and the routine steps to the next one. However, if the difference between the two is π or greater, then multiples of 2π or -2π are added to the second pixel until the difference is less than or equal to π. The routine then steps to the next pixel and the process is repeated. If all pixels are valid and there are no discontinuities such as a strong shock wave, this process is very effective.

The difficulty of creating a phase unwrap for images collected in the lab occurs from the fact that the images collected are two dimensional and there are extreme amounts of noise in the images. A modification of the one dimensional unwrap routine was attempted. In this routine, the upper corner of the image was chosen as the starting point and the phase was unwrapped along a line across the top of the image. Once this line was unwrapped, the one dimensional unwrap was utilized along each

column in the image. For an ideal image, this process should work effectively, but a single noise pixel in a column propagates the noise throughout the entire column, thus invalidating the bottom portion of the image.

An attempt was made to determine an algorithm that would utilize the knowledge given by the entire image. The two dimension unwrap is easily accomplished by a human examining the image, but the difficulty comes from automating the process. Any routine designed to examine the full two dimensional field must also be capable of unwrapping around any noise pixels without the errors propagating throughout the entire image.

Determination of Regions

The concept finally chosen was to divide the entire image into regions of like phase. Before the pixels are divided into the regions, they are assigned a trigonometric quadrant number corresponding to the values of phi at each point, i.e. quadrant #1 contains all pixels with a value between 0 and $\frac{\pi}{2}$, quadrant #2 contains all pixels with a value between $\frac{\pi}{2}$ and π, etc. Once all of the pixels are tagged with the numbers 1, 2, 3, or 4, the groups of pixels are then placed into regions. All touching pixels with the same tag number are assigned to a single region. Once every pixel is placed in a region, the region grouping routine is complete and records the number of regions formed, the number of pixels in each region, and the column number of the first pixel in the region. The program then begins the actual unwrapping of the regions.

This concept is shown in Figures 14 and 15. The region classifications have already been performed by the first block of these figures. The routine begins in the upper left hand corner of the image and sets the corner pixel as being in region #1. Then it progresses by first stepping down through a column and then moving over a column and repeating the process until the whole image is unwrapped. In the given figures, the pixel directly below already set region #1 is of a different quadrant, so it is established as region #2. Since all of the pixels below this one are all of the same quadrant, the rest of the column is tagged as region #2.

The code then begins the region checking at the top of the second column. Since this pixel is within the same quadrant as the pixel to the left, it is also tagged as being part of region #1. This continues down the column until it hits the sixth point. This point is not within the quadrant of either the pixel above it or to the left of it. Since neither side of it fits the required parameters, this becomes a new region which is numbered region #3.

This routine progresses smoothly until region #5 is hit. The first pixel tagged as region #5 is directly below the farthest right point of region #1. When the code completes that column and begins grouping the next column, the top pixel should be grouped with region #5. However, since the code can only check the pixel directly to the left, and gives it a different number than region #5, instead it is assigned region #6. The pixels directly below it are also assigned to region #6 until the pixel directly next to region #5 is encountered.

When this pixel is checked, the code determines that the pixels both above and to the left are of the same circle quadrant, but they are assigned to different regions. The code then places all of the pixels in region #5 and region #6 into the same region. In an attempt to save computing time, the smaller of the two regions is grouped into the larger of the two. Therefore, the pixel in region #5 is placed in region #6. The code then continues its sweep of the entire image.

The main drawback of this routine is the creation of many regions that contain 0 pixels when the routine is complete. If the fringes are diagonal upwards to the right, there can be as many as 90% or more of the created regions without any pixels. In an attempt to correct this to reduce memory used and time required in future steps, another routine was developed to renumber the regions. This routine just steps forward in region numbers and checks to see if it has any pixels in it. If it does, then the region number is given a new number in such a way that the regions are number sequentially with all of the regions being valid, i.e. having pixels assigned to that region. The result of this routine is shown in the first diagram in Figures 14 and 15 with the regions numbered in order with no numbers missing.

Spiral Method

Various unwrap techniques were attempted using the region method. The most difficult problem with the unwrap was to develop a routine that would allow for the image to be unwrapped without sensitivity to the starting point location. Originally,

a spiral pattern unwrap process was implemented. An example of this process is displayed in Figure 14.

For the spiral method, the user selects a starting point by clicking on the interferogram that is displayed on the screen. In the example shown in Figure 14, the first diagram shows the point selected by the user; the point located in region #3 which is highlighted. Once this point is selected, the entire region #3 is established as being unwrapped without being altered.

Now, the spiral begins checking the pixel directly above the selected starting point. Since this pixel is also within region #3, the method checks the pixels to the left until it is one pixel to the left of the left-most checked area. In this case, it is the pixel right next to the one it just checked. This pixel is also in region #3, so it is also unchanged. The code then checks each pixel below this point until the pixel being checked is one below the bottom pixels in the checked area.

In this case, all of the pixels are located in region #3, so nothing happens at these points. The code then begins checking to the right along this row until it is one pixel farther right than the right-most checked area. However, in this example, the point directly below the selected pixel is part of region #4, which has not been unwrapped.

Now, region #4 must be unwrapped based on its neighboring unwrapped regions. The code steps along every point located in region #4 and checks to see if there are any points neighboring it of a different region that have been unwrapped. If the pixel borders any non-diagonal unwrapped pixels, the code determines the shift required in

ϕ to bring the two regions within $\pm\pi$ by adding or subtracting 2π. In later stages of the unwrap, noise may cause an inconsistent phase shifting required. If this happens, the required shift with the largest number of pixels is used and the discontinuity is created only on the smaller border. In the case of the second region being shifted, the only unwrapped border is with the original region, so the shift must be consistent.

After a required shift is determined, all pixels located in the given region are shifted by an equal amount. In this case, all pixels in region #4 are shifted by the required multiple of 2π and established as unwrapped. Once the entire region is unwrapped, the code continues stepping. The pixel directly next to the point used in the last shift is of region #5, which has not yet been unwrapped.

Now, the code once again examines all of the pixels located in region #5 and checks to see if there are any unwrapped pixels neighboring it. In this case, there are three pixels from region #3 and only one pixel from region #4. The code checks to determine the required shift to bring regions #5 and #3 to within $\pm\pi$ and then checks to see the shift required to bring regions #5 and #4 to within the same range. If the multiples of 2π required to bring the pixels within the required ranges is consistent between both borders, then region #5 is shifted by that amount and is unwrapped. If there is an inconsistency, the more common of the two shifts is used. In this case, the shift required by the border with region #3 is used since the border pixels in region #3 outnumber those from region #4.

Once the pixel to the right of the right-most checked area is reached, the code begins to step upwards checking the pixels until the topmost checked row is reached. Once this row is reached, the code steps leftward until the box is complete with the starting point in this iteration. Then, the code steps one more pixel directly above the starting point and begins another box iteration.. As can be seen in Figure 14, this process continues until every pixel in the image is checked.

For a perfect image, this routine should have difficulties only in regions with discontinuities such as a strong shockwave. From observations of the Mach 6 test data, the shift caused by the shockwave was not large enough to cause a discontinuity greater than an entire fringe between any two pixels of the finite interferogram. The problems encountered with this routine are caused by noise in the images, especially when noisy pixels are encountered early in the spiral. If the user clicks on a noisy pixel, or if one of the first few regions encountered are noise, then the shifting of neighboring points can be greatly influenced because the larger non-noisy regions have not been unwrapped yet, and therefore are unable to influence the shifting required. Once an error in the required shifting is established, this error tends to propagate into the surrounding regions. Tests of this routine showed it to be very sensitive to the starting pixel location, and thus to the point chosen for the unwrapping. An attempt was made to correct this problem using a different unwrap routine.

Largest Neighbor Method

The region selection appeared to eliminate most of the noise in the image, so the new unwrap routine was designed to fully utilize the region grouping concept. The routine was designed to attempt to reduce any unwrap errors caused by unwrapping a small portion of the image that is touching the chosen point rather than using the larger border with a different region. This routine unwraps the image using a two step process after the pixels are grouped by region.

The first step in the unwrap procedure is to determine the "largest neighbor", i.e. the region containing the most adjacent pixels, for every region located in the image. To perform this task, the routine selects each region in order of region number, then checks every pixel in that region to determine the regions adjacent to a given pixel. A marker is used to ensure no neighboring pixels are counted twice in areas containing region corners. Once all of the neighboring regions are determined, the three largest neighboring pixels are stored in arrays to be used in the next step of the process. In Figure 15, the code first attempts to determine the "largest neighbor" for region #1. An examination of the image shows that it borders region #2 with 4 pixels, region #3 with 4 pixels, and region #5 with 4 pixels. Usually, the largest three neighbors are stored in descending order, but all three of the neighboring regions in this image have the same number of border pixels. Therefore, the code stores the largest neighbor in numerical order, causing region #2 to be the largest neighbor and region #3 to be the

second largest neighbor. The routine then moves to the next region and determines the largest neighbor for this region.

After all of the largest neighbors have been tagged for every region, the second step of the unwrap process begins. The starting point for this step was chosen to be the region containing the most number of pixels. In Figure 15, region #1 is the largest with 20 pixels located in the region. This entire region is flagged as unwrapped. The routine then begins checking all of the other regions to see if the unwrapped region is the largest neighbor to any of them. If a region is found, a pixel in each of the bordering regions is selected arbitrarily to determine the required shift value in multiples of 2π to insure the difference between the pixel values is less than π. Every pixel in the region is shifted this required amount, and the region is flagged as unwrapped.

The routine proceeds by checking if there are any other regions which have their largest neighbors already unwrapped, thus allowing further unwrapping of the image. After one pass is completed, the routine checks every unwrapped region for the largest neighbors to check if any further unwrapping can be accomplished. If more regions are found, the routine continues looping through all of the regions until it either unwraps all of the image or is unable to find a region having its largest neighbor unwrapped. If it encounters the latter condition, the routine then looks at the second largest neighbor and attempts a pass through all of the regions. Now, if a region is found with the second largest region unwrapped, the routine unwraps the region in question

and returns to iterating on the largest neighbor. If an entire pass is made without finding a region unwrappable from the second largest region and there are no valid points, then the routine is forced to drop down to the third largest region. Again, once a valid region is determined and shifted, the routine returns to checking for the largest neighbors. If, however, there are no valid third largest neighbors, the unwrap routine terminates and the overall program continues. The third largest neighbor was decided as the lowest level checked because using any smaller neighbors would cause the routine to be more sensitive to noise. The majority of the images examined are able to be completely unwrapped with this method, while the image exhibiting small unwrap problems have over 90% of the image unwrapped.

This routine is very insensitive to noise because small regions have very small effects on the larger regions. Using the largest neighbor causes the unwrapping of the undisturbed area to be consistent, which was not the case for the spiral method.

Figure 15 is a good example of the progression of the unwrap. Once region #1 is tagged as the largest, the code steps through the rest of the regions in numerical order to see if region #1 is the largest neighbor for any of them. In this case, region #2 has region #1 as its largest neighbor, so region #2 is unwrapped off of region #1. Since region #2 is now unwrapped, the code continues through the iteration, now checking to see if region #1 or region #2 is the largest neighbor to any other region. Since this is not the case, the iteration is complete without unwrapping any other pixels. Now, the code begins with region #1 and begins the second iteration. If a

region has been already unwrapped, it is skipped in the iteration. With this pass, no regions were able to be unwrapped, so the code begins stepping through the regions looking for a second largest region. Stepping through, region #5 is determined to have region #1 as its second largest neighbor. Region #5 is then unwrapped off of region #1. Instead of continuing this iteration, the code now begins checking for the largest neighbor again starting at region #1. Once again there are no regions with an unwrapped region as its largest neighbor, so the code begins looking for the second largest region.

Region #3 has region #5 as its second largest region, so region #3 is unwrapped from region #5. The iteration begins again looking for the largest region, and region #4 is determined to have region #3 as its largest region, so region #4 is now unwrapped. The code continues to search for any largest neighbors in this iteration touching any unwrapped points. Since this is not the case, the code begins the next iteration.

Once again, this iteration fails to have any wrapped regions with an unwrapped largest neighbor. Using the second largest neighbor again, region #6 can now be unwrapped using region #5. The iteration beings again looking for the largest neighbor, and region #7 is determined to have region #6 as its largest neighbor. With the unwrapping of region #7, the image is completely unwrapped and the data reduction software can continue.

Removal of Reference Fringes

After the unwrapping is completed, the image now has all 2π ambiguities removed, except for the finite fringe phase maps, the process is not finished yet. For the finite fringe maps, an image appears to have a phase that is changing in the undisturbed region of the flow corresponding to the reference fringes. Since for a correctly reproduced image the fringes in the undisturbed flow are straight, a subroutine is then used which will eliminate the effects of these reference fringes. Since the fringes are assumed linear, the change in fringes can be broken into the row and column components. Each of these components are subtracted across the entire image, and because of the linearity of the fringes, the order of subtraction has no effect. Once these reference fringes have been eliminated, the unwrap of the image is complete.

Comparison of Unwrap Methods

Both of the previously mentioned methods, spiral unwrap and largest neighbor unwrap, should perform well for a given image. Both of the routines produce fairly clean unwrapped phase maps of a flow without the 2π ambiguities or reference fringes. There are benefits and disadvantages to both methods, providing the rational for the user choosing between the two methods during the unwrap portion of the data analysis.

The main advantage to the spiral method is the speed by which the routine performs the unwrap. The speed of the spiral method outweighs the sensitivity of

this method to the unwrap starting point location and noise within the image. For most images, the spiral unwrap method produces an unwrapped phase map that can be used for qualitative analysis of the flow. Figure 16 shows an example of an unwrapped candle flame using this method. This image provides a clear view of the candle flame even though there are errors in the unwrap because of sensitivity to noise. These errors are manifested in the diagonal streak in the upper center of the image.

The largest neighbor method trades the speed achieved with the spiral method for a better, more accurate view of the flow. Figure 17 provides a better unwrap of the candle flame than the spiral method. The drawback of this method is the increase of computational time, which increases with the number of regions rather than the image size. The spiral method speed is primarily related to the image size because of the methodological method of unwrapping. The iterative logic of the region method causes the speed to be more directly related to the number of regions. The trade-off between the two unwrap methods is simple speed versus performance. If the image contains a substantial amount of noise, the method to use would be the largest neighbor method. Unfortunately, by using the largest neighbor method, the computational time increases. Now, if the image contains little to no noise, the better method to use would be the spiral method since computational time can be decreased without a significant loss in unwrap performance.

In an attempt to further improve both methods, it was decided to break the circle into more than the four sections mentioned earlier. Splitting all of the four quadrants in half led to a method which divides the trigonometric circle into eight equal regions. This should produce a large increase in the number of regions created, but should also provide for a more flexible unwrap since fewer pixels are grouped together. For images which contain a lot of noise, this increase in the divisions produces far clearer results. In the case of the candle used to demonstrate the differences in the unwrap methods, using the eight sections provides very little added benefit since the image is fairly clean. In fact, for the case of the spiral method, the eight division method produces a poorer image as shown in Figure 18 than that of the four division method. The region method produces a slightly improved phase map, with the improvements appearing in the actual candle flame. This method provides a greater resolution as shown in Figure 19. The limited resolution of the laser printer fails to adequately display the differences between the two.

QUALITATIVE RESULTS

With the data reduction software was complete, a qualitative analysis of any interferogram can be achieved with minimal effort. All of the interferograms mentioned above were able to be reduced to a phase map with all of the 2π ambiguities removed.

After the candle was used as a simple example for development purposes, the next image attempted to be unwrapped was the heat pattern produced by a heat

gun. A heat source was once again chosen because a highly varying density field is easily created through the use of heat. Figure 20 is the final qualitative analysis of this flow using the largest neighbor unwrap dividing the circle into eight regions. As can be seen, the area outside of the flow appears as a relatively flat field. The jet begins with a clear core flow and then becomes turbulent as it progresses.

The poor quality of the Mach 3 wedge holograms provided the greatest challenge to the unwrap software. In an attempt to improve the unwrap without drastically increasing computational time, only a small section of the wedge was used in the analysis. As show in Figure 21, the unwrap of this small section produces an excellent view of the flow. The freestream is a flat field with a phase ϕ of 0. The theory for a wedge flow predicts that the flow parameters inside the shockwave are constant, so, the density through the area should be a flat field with $\phi > 0$. This is clearly seen in the image, so qualitatively, the phase is exactly what is expected.

The Mach 6 cone test was expected to provide results allowing the examination of the boundary layer. Problems with the two beam alignment mentioned in the single plate method , erroneous signal beam/reference beam ratios and incorrect photographic development procedures, produced poor quality holograms for this examination. A good qualitative view of the flowfield was able to be produced despite these problems, as seen in Figure 22. The corners of the flowfield are very noisy because that portion of the image was clipped during the reproduction and capturing of the images. Therefore, this area contains only noise and no data. The freestream

contains the lowest density of the image, and thus is a flat black field. The shock-wave is clearly exposed by unwrapping the image and removing the reference fringes. Finally, the boundary layer is evident close to the blacked out model.

The final images examined for qualitative analysis were the blowing jets of various backpressures. For the case for a backpressure of $273kPa$, the unwrap of the jet is shown in Figure 23. In this image, the background is a flat field. The area of the jet flow is shown as the lighter region because the density of this area is higher than that of the surrounding area. The small size of the nozzle prevents the structure of the flow from being seen clearly.

An unwrap was attempted for the case of a backpressure of $446.1kPa$. This flow produces too strong of a density increase causing the fringes to become discontinuous. The program is unable to unwrap any images with discontinuous fringes. Because of this difficulty, the unwrap was not attempted for the higher backpressure.

CHAPTER V

QUANTIZATION OF DATA

Once an image has been correctly unwrapped, the actual quantization of the data can be performed. This process has been well established by a variety of researchers.[8]

THEORY

As collimated light passes through a disturbed flow, the light ray paths are altered as a function of the disturbances, causing changes in the phase of the light visible in the unwrapped phase map. The two major disturbances of interest are density changes and ionization of the medium, measured by the amount of free electrons. The refractivity of the light through a region of free electrons is very wavelength dependent, but the refractivity through a density field is almost completely wavelength independent. Thus, both the density and the ionization of a flow may be determined simultaneously through the use of two different wavelengths.[12] For the test conditions observed in the experiments performed at Wright-Patterson AFB, the ionization of the flow is negligible, so only one wavelength is required to perform a density measurement.

The first step in converting the unwrapped phase map into a density map is the transformation of the phase map into an index of refraction map. For two dimensional or axisymmetric images, this can be done easily. However, for a three dimensional

disturbance, tomography is required using multiple images at various viewing angles.[13,14] However, for the interferometer system used at Wright-Patterson, only one image view was available, limiting the system to two dimensional or axisymmetric disturbances.

The conversion of a phase map into an index of refraction map for the two dimensional case is described in Vest.[8] The general equation for the conversion of phase into index of refraction is given as:

$$\Delta\Phi = \int [n(x,y,z) - n_o] = N\lambda \tag{5.1}$$

where n_o is the index of refraction of the region during the reference shot, N is the phase number, and λ is the wavelength of the light used to probe the area. The conversion from the Φ in Equation 5.1 relates to ϕ calculated from Equation 2.4 by

$$\Phi = \frac{\lambda}{2\pi}\phi \tag{5.2}$$

Equation 5.1 then becomes

$$\Delta\phi = \frac{2\pi}{\lambda}\int [n(x,y,z) - n_o] = 2\pi N \tag{5.3}$$

For the two dimensional case, the index of refraction of the disturbed image is only a function of x and y, so Equation 5.3 becomes

$$\Delta\phi = \frac{2\pi}{\lambda} L\,[n(x,y) - n_o] \tag{5.4}$$

It follows that the index of refraction at a given point can be calculated by

$$n(x,y) = \frac{\lambda}{2\pi}\frac{\Delta\phi}{L} + n_o \tag{5.5}$$

where L is the phase object length. This calculation is performed throughout the entire image. Since the index of refraction calculation at each point depends only on the phase value, length of the test section and the original index of refraction, the calculation is not order-oriented. So a simple loop is performed in the program analyzing the entire image one row at a time until all of the rows have been calculated.

The axisymmetric case is more difficult because a line of sight integration is performed throughout the image. Equation 5.1 becomes, for the axisymmetric case,[8]

$$N(x) \cdot \lambda = 2 \int_x^R \frac{(n_r - n_c) \cdot r \cdot dr}{\sqrt{r^2 - x^2}} \tag{5.6}$$

where r is the radius from the model centerline, R is the radius of the entire axisymmetric phase object. Equation 5.6 can be rewritten, for disturbances without discontinuities which decay to zero far away from the object, as

$$N(x) \cdot \lambda = 2 \int_x^\infty \frac{(n_r - n_o) \cdot r \cdot dr}{\sqrt{r^2 - x^2}} \tag{5.7}$$

with the right hand side of the equation being an Abel transform of $(n_r - n_o)$. Therefore, using the Able transform inversion, Equation 5.7 becomes,

$$(n_r - n_o) = -\frac{\lambda}{\pi} \int_r^\infty \frac{(dN/dx) \cdot dx}{\sqrt{x^2 - r^2}} \tag{5.8}$$

An assumption must be made to utilize Equations 5.7 and 5.8 since the data is known only at discrete points rather than throughout the entire field. Because the data is known at each pixel location and each pixel corresponds to about $\frac{1}{100}$ of an inch for the images acquired from the wind tunnel test, it was assumed that the density

is constant throughout each pixel. Discretization of Equation 5.7 leads to a set of simultaneous linear equations defined by the summation

$$\sum_{k=i}^{I-1} A_{k,i} \cdot (n_k - n_o) = \frac{\lambda}{4\pi} \frac{\Delta\phi_i}{\Delta r} \tag{5.9}$$

where $A_{k,i}$ is defined as

$$A_{k,i} = \left[\sqrt{(k+1)^2 - i^2} - \sqrt{k^2 - i^2} \right] \tag{5.10}$$

Using Equation 5.9, n_r may be determined with the calculations performed from the outer point inward until the model surface is reached. This calculation must be performed for every line of pixels perpendicular to the model centerline. For the calculations made in conjunction with tests performed at Wright-Patterson, the model centerline was aligned vertically on the images, so the calculation was simplified by each row being independent of all others. The calculation was performed from the top of the image down to the bottom, but the order of calculations was irrelevant.

Once the index of refraction map has been calculated by either Equation 5.5 or Equation 5.9, depending on the disturbance being examined, the density can be calculated. According to Vest,[8] the density can be related to the index of refraction change by the Gladstone-Dale equation:

$$n - 1 = K\rho \tag{5.11}$$

where K is the Gladstone-Dale constant, and n is a function of the wavelength of the light used. The Gladstone-Dale constant is only a weak function of the wavelength,

and independent of temperature and pressure for the conditions examined. For the wavelength of the Ruby laser, the value of the Gladsone-Dale constant is $0.0002251\frac{m^3}{kg}$ for air. The density of the disturbed object can be calculated as

$$\rho(x,y) = \rho_o + \frac{n(x,y) - n_o}{K} \tag{5.12}$$

where ρ_o is the density known from the reference condition. The value of n(x,y) need not be explicitly calculated in Equations 5.5 and 5.9 since the term $n(x,y) - n_o$ is present in Equation 5.12. Also, as a result of the presence of the term $n(x,y) - n_o$, the exact value of n_o need not be known.

QUANTITATIVE RESULTS

Once the equations for the conversion from ϕ to density were established, it was easy to develop a computer code to calculate the density for a flowfield provided that it was two-dimensional or axisymmetric. After this was coded, an attempt was made to determine the density for the unwrapped phase maps of the Mach 3 wedge flow, the Mach 6 cone flow, and the small nozzle.

Mach 3 Wedge

The first attempt at validating the quantization routines was made using the 10° half-angle Mach 3 wedge because it is a simple two dimensional flow. The stagnation conditions lead to a stagnation density, ρ_o, of 14.214 $\frac{kg}{m^3}$. From the isentropic flow tables for supersonic flows,[15] the freestream density ρ_∞ is calculated to be 1.0835 $\frac{kg}{m^3}$.

Using this density as the freestream density, standard oblique shock analysis[15] shows that the flowfield inside the shockwave should be constant. Using the oblique shock tables,[15] the density ratio between the density inside the shock wave to the freestream shockwave is $\frac{\rho_2}{\rho_\infty} = 1.655$. This leads to a density inside of the shockwave of $1.793\frac{kg}{m^3}$.

A small clip of the Mach 3 wedge flow was used in an attempt to determine the density inside the shockwave. Figure 24 shows the density calculated through the use of the data reduction software. The density inside of the shockwave is seen to be $1.1124\frac{kg}{m^3}$. This value leads to an error of over 35% from the correct answer. An attempt was made to determine the source of this large error.

It was decided to take the analytic result and determine the phase shift required to produce that change in density. The required change in density is $0.710\frac{kg}{m^3}$. Using Equation 5.12, the change in index of refraction can be determined to be

$$n(x,y) - n_o = K\Delta\rho = 0.0001598$$

Once the change in index of refraction is determined and rearranging Equation 5.5, the required $\Delta\phi$ can be determined as

$$\Delta\phi = \frac{2\pi L}{\lambda}\Delta n = 183.7$$

this $\Delta\phi$ leads to a phase shift of 29 fringes. Since the shockwave is very small in width, this change of 29 fringes must occur within a region of only a few pixels. The fringes become discontinuous as they cross the shockwave, so the code misidentifies the shift to be under 4π. Without entering the density within the shockwave into the data reduction software, the current system is unable to cross such a strong discontinuity.

Mach 6 Cone

Since the equations for the quantification of the data depends on the absolute change in density, it was hoped that the density could be accurately calculated in a flowfield with both a lower freestream density and a weaker shockwave. The Mach 6 wind tunnel operates at static conditions much lower than those of the Mach 3 wind tunnel. The static density for most of the data shots taken in the cone test was $0.1703\frac{kg}{m^3}$. This is a reduction of almost 85% from the density of the Mach 3 wind tunnel. It is believed that this reduction along with a smaller half-angle and an axisymmetric flowfield would allow the correct density to be determined.

First, the expected density was calculated for the flowfield. A Taylor-Maccoll solution was performed using a computer code supplied with a compressible fluid dynamic textbook.[15] This solution is an inviscid solution to the flowfield, but will apply to the flow away from the boundary layer. The density at the shockwave was determined to be $0.2598\frac{kg}{m^3}$. This density leads to a near-surface density of $0.2950\frac{kg}{m^3}$. This density should be valid just outside of the boundary layer for the flow.

Using Equation 5.9 and the methods described above, the density can be determined from the phase map created by the data reduction code. This analysis depends heavily on the centerline and the pixel dimensions selected earlier. The density calculated through the use of this code is shown in Figure 25. As expected, the freestream is a flat field with the density of about $0.1703\frac{kg}{m^3}$. Since the freestream density was an input into the code, this result is expected. Using only the method for calculating an

axisymmetric flowfield, the computer code calculated the density within the shockwave. The density just inside of the shock was calculated to be around $0.26\frac{kg}{m^3}$. Noise in the flow and the large amounts of noise in the corners cause the actual values of the density to vary slightly, but all of the pixels are close to the analytic value.

This solution quickly deviates from the expected values as the density was calculated closer to the body of the model. At the point just outside the boundary layer, the density was calculated to be around $0.4\frac{kg}{m^3}$. This gives an error of over 35%. Since the density was accurately determined just inside the shockwave, the shockwave strength cannot be the explanation of the density errors.

The source of these errors can be seen clearly in the phase map of the cone given in Figure 22. A ring pattern is clearly visible within the shockwave. Since these rings are not evident in the Mach 3 phase maps or the phase maps of the images taken in the lab, it is believed that the source of these errors is the wind tunnel itself. The Mach 6 produces a conical flow rather than the two-dimensional flow of the Mach 3 facility. Since the core of the flow is larger than the windows on the side of the tunnel, there is no light passed through the tunnel outside of the conical flow. Since the freestream now has a change in index of refraction because the tunnel density outside the core flow is much greater than that inside the core flow, there is no region of straight reference fringes, greatly complicating alignment. Added to this difficulty of aligning the holograms are the errors associated with the single plate method alignment, causing the plate to be rotated in order to align the holograms.

It is believed that the combination of these two error sources have caused the images to not be accurately aligned, causing the rings in the flowfield phase map.

Jet Flow

The final attempt at validating the Holographic Interferometry system was made using the images of the jet flow taken in the laboratory. The primary difficulty with these images is the small size of the nozzles.

An engineering analysis was made to provide the expected results. Using common analysis techniques for an underexpanded jet,[16] the density field was able to be calculated. This analysis is shown in Figure 26 for a stagnation pressure of $273.7kPa$. Since the ratio of this pressure to atmospheric pressure is greater than the 1.893 for Mach=1 and the exit of the nozzle is the smallest area of the flow, the flow at the exit plane must be choked. Using the isentropic flow tables,[15] the static pressure at the exit must be $144.6kPa$. More importantly, the density can be calculated from the given conditions. With the storage vessel for the high pressure air kept at room temperature, the stagnation density becomes $3.295\frac{kg}{m^3}$. Using the isentropic flow tables for M=1, the static density at the exit can be determined to be $2.09\frac{kg}{m^3}$. The density in region #3 shown in Figure 26 then becomes $0.40331 \times \rho_o$. This density is $1.33\frac{kg}{m^3}$.

As seen in Figure 27, the structure of the flow from the jet is very difficult to see. However, the density at the exit is around $2.0\frac{kg}{m^3}$ which is what was calculated in the analytic solution.

CHAPTER VI

CONCLUSIONS

Several conclusions can be made from the work performed at Wright Laboratory in an attempt to advance the Holographic Interferometry system. The single plate and the dual plate interferometry systems were examined. Both of these methods possess advantages and disadvantages.

The single plate system provides the advantage of using only one plate for both the reference and signal shots. This reduces the total number of plates required for a test and reduces the amount of work required with placing and removing the holographic plates. The phase-shifting of the interferograms is also simple because there are two separate beams used. One pathlength of one of the two beams can easily be changed using a piezoelectric mirror. A portion of both beams can be split and interfered with the other beam allowing the exact shifts to be easily known. Using the pathlength difference to shift the fringes, however, produces problems with vibrations. The interferograms are not very stable and tend to be very sensitive to very small vibrations in the room. The alignment of the reference laser beams in the recorder is also very difficult. Using an alignment hologram, this alignment problem can be reduced.

The dual plate system is an easy system to align. Since two different plates are being used, only one reference beam is used. The reader system is also greatly

simplified because only one leg is required. This also allows for a brighter reproduction of the hologram because the reproduction beam is not split. The main disadvantage of the dual plate system is the difficulty with the phase-shifting. The fringes are very stable in this system because the fringe spacing is dependent on the spacing between the two plates. Using a rotation stage, this spacing can be altered giving the required phase shifts. However, since there are not two beams to interfere, the only visible interference is from the two holograms, so the actual images must be examined to determine the required rotation rather than a piece of each beam as used in the single plate method.

Two different unwrap methods were developed to allow for unwrapping of noisy images. These two methods are the spiral method and the largest neighbor method. The main advantage of the spiral method is relative speed at which it unwraps an image. This routine is faster than the largest neighbor region and produces adequate results for clean images without noise or speckle. The largest neighbor region produces excellent unwraps of the phase maps even for poor images. However, the speed of this method is dependent on the number of regions, thus the very noisy images require large amounts of time.

The quantification of the results from the wind tunnel test data proved to be more complex than originally believed. Both the Mach 3 wedge and Mach 6 cone test data produced erroneous measurements because of difficulties encountered associated with the actual physics of the flows being investigated. The Mach 3 wedge data

could not be analyzed correctly because the shockwave is strong enough to produce a discontinuous phase shift of 29 fringes which can not be tracked by the software. The Mach 6 cone data produced improved results. The density calculated just inside of the shockwave was accurate, but the alignment problems associated with the single plate method and the conical flow of the Mach 6 wind tunnel, caused the errors in the calculated density to increase towards the model. The best results were produced from the jet flow interferograms. The density map appeared to be correct, but the small size of the jet nozzle prevented a detailed analysis of the flow structure.

RECOMMENDATIONS

The success of the Holographic Interferometry system depends on the data reduction software accurately calculating the phase-shift of a flow. This software is unable to reduce the data for images where there is a discontinuity in phase. For these cases, such as the Mach 3 wedge flow used in this research, the data can still be reduced by assuming the value of the density just inside of the shockwave and then allowing the data reduction to proceed towards the model.

The other major source of error encountered upon tunnel entry was the problem of an axisymmetric open jet tunnel such as the Mach 6 facility. This becomes a major source of error because the data reduction algorithms assume the integrated density across the tunnel to be constant in the area outside of the shockwave. The axisymmetric open jet produces a flow where this is not true, and the area outside of the jet, where this is valid, is not viewable. The solution to this problem is to

remove the effects of the jet flow by recording the reference hologram with the tunnel running and the model removed from the flow. Obtaining the reference hologram in this manner would eliminate the curvature of the fringes in the interferogram caused by the tunnel flow and the data reduction could be accurately performed.

BIBLIOGRAPHY

[1] B.M. Watrasiewicz and M.J. Rudd. *Laser Doppler Measurements.* Butterworths & Co., Boston, MA., 1976.

[2] Anthony O'Keefe. Hypersonic flow diagnostic development. Technical Report WL-TR92-3034, Wright Laboratory, 1992.

[3] Charlie Tyler. *Development, Analysis and Application of Laser-Induced Fluorescence and Rayleigh Scattering Measurement Systems in a Hypersonic Wind Tunnel.* PhD thesis, University of Dayton, 1996.

[4] Thomas J. Beutner, et al. Doppler global velocimetry measurements of a vortex-tail interaction. In *Flow Visualization VII Proceeding of the Seventh International Symposium on Flow Visualization*, pages 418–423, September 1995.

[5] Mark S. Maurice. *An Investigation of Laser Velocimetry Measurements Within High Speed, Complex Flows.* PhD thesis, University of Dayton, 1992.

[6] Bustusov M.M. Ostrovsky, Yu.I. and Ostrovskaya G.V. *Interferometry by Holography.* Springer-Verlag, Berlin, 1980.

[7] Linda G Smith, Charles Tyler, and John D. Schmisseur. Advanced diagnostics research for high speed aerodynamic testing. In *Aerotech '92 SAE Technical Paper Series*, 1992.

[8] Charles M. Vest. *Holographic Interferometry.* John Wiley & Sons, New York, 1979.

[9] K. Creath. Phase-measurement interferometry techniques. *Progress in Optics*, 26:349–393, 1988.

[10] A. George Havener. A users guide on pulse laser holography for wind tunnel testing. Technical Report ARL-TR-75-0213, Aerospace Research Laboratories, 1975.

[11] T.A.W.M. Lanen. Digital holographic interferometry in flow research. *Optics Communications*, 79(5):386–396, 1990.

[12] F.H. Oertel and J.H. Spurk. Two-wavelength laser interferometry of hypersonic ionized flows. In *ICIASF '69 Record*, 1969.

[13] Arthur J. Decker and Steven H. Izen. Three-dimensional computed tomography from interferometric measurements within a narrow cone of views. Technical Report 103257, NASA, March 1991.

[14] Charles M. Vest. Tomography for properties of materials that bend rays: A tutorial. *Applied Optics*, 24(23):4089–4094, December 1985.

[15] B.K. Hodge and Keith Koenig. *Compressible Fluid Dynamics With Personal Computer Applications.* Prentice Hall, Englewood Cliffs, NJ, 1976.

[16] Robert D. Zucker. *Fundamentals of Gas Dynamics.* Matrix Publishers, Chesterland, OH, 1977.

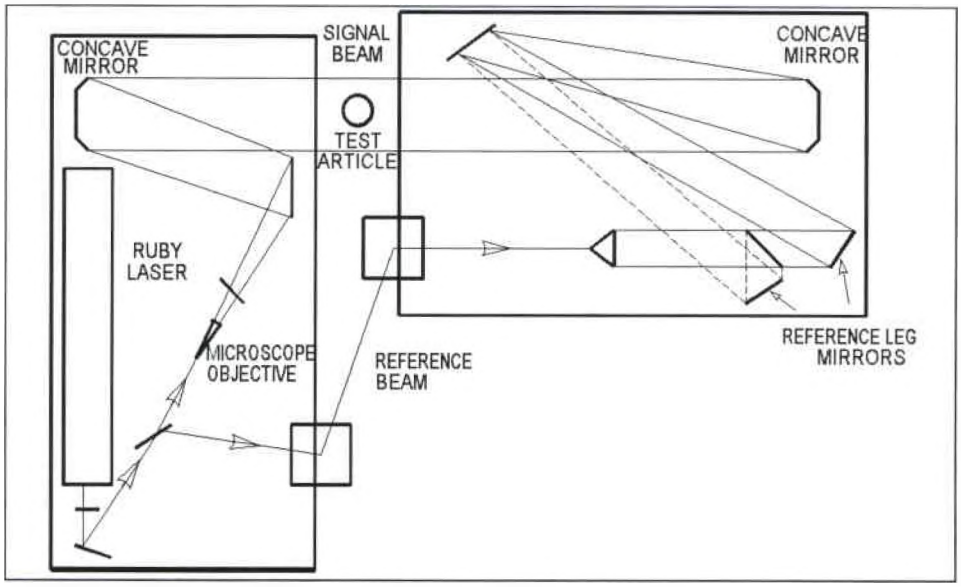

Figure 1: Holographic Interferometry Recorder System

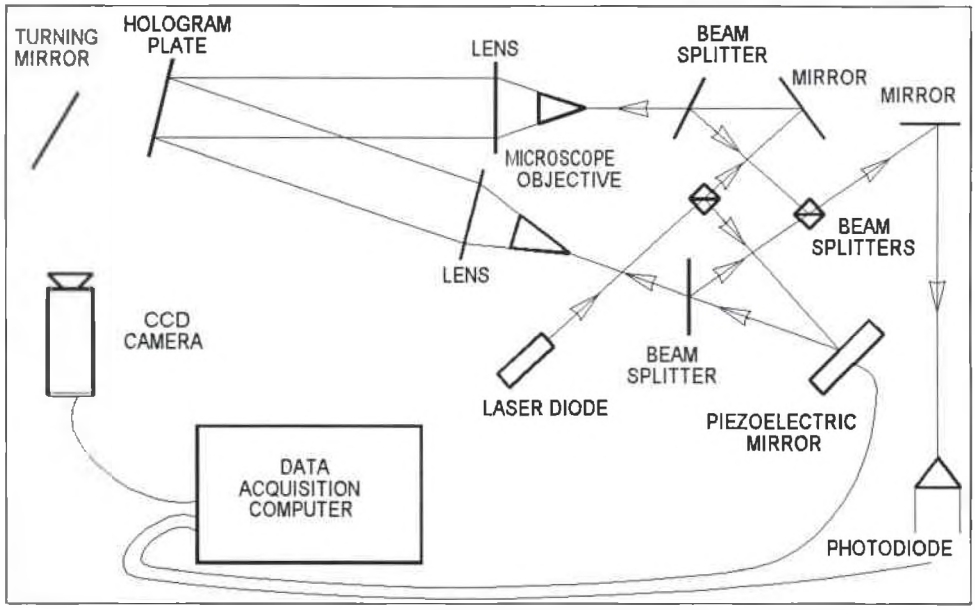

Figure 2: Holographic Interferometry Reader System

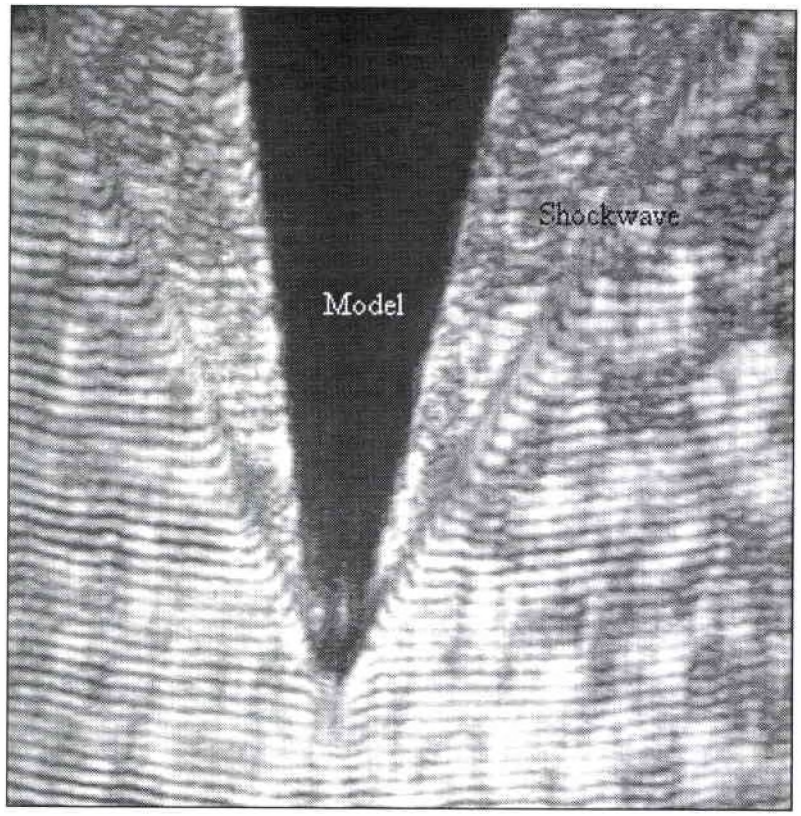

Figure 3: Interferogram of Wedge at M=3

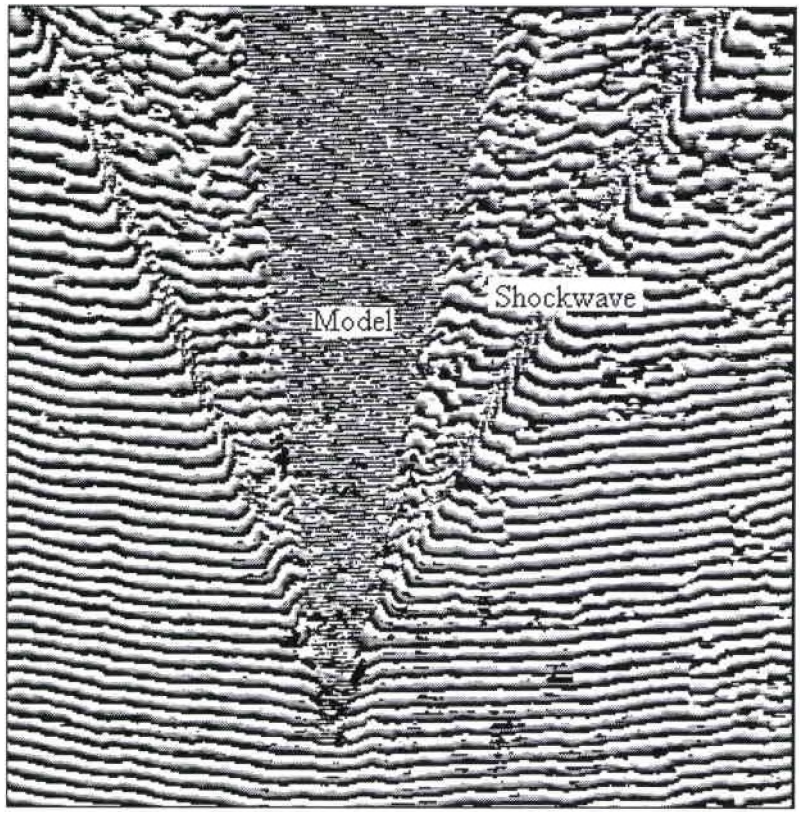

Figure 4: Phase Map of Wedge at M=3

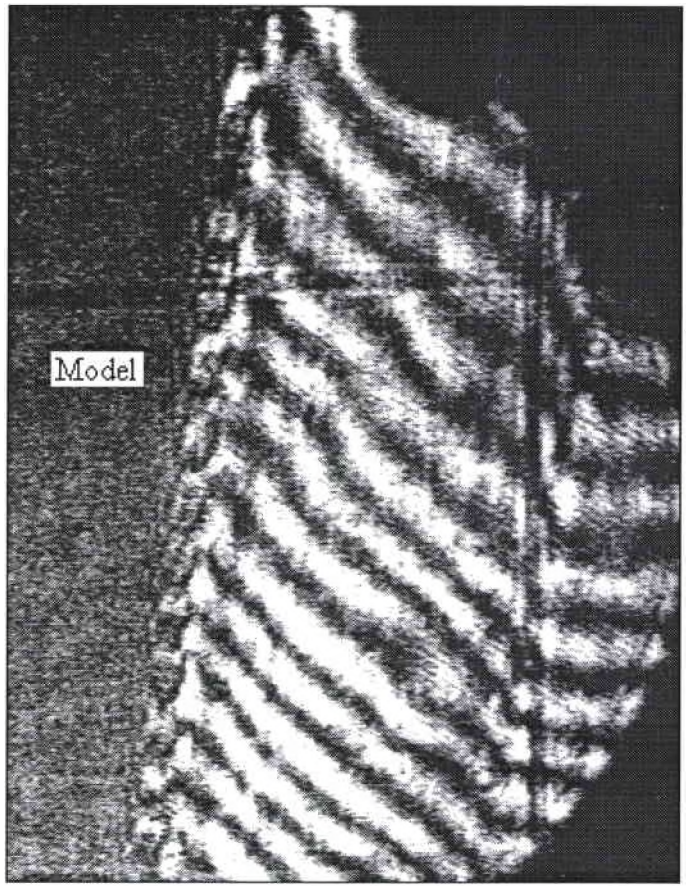

Figure 5: Interferogram of Cone at M=6

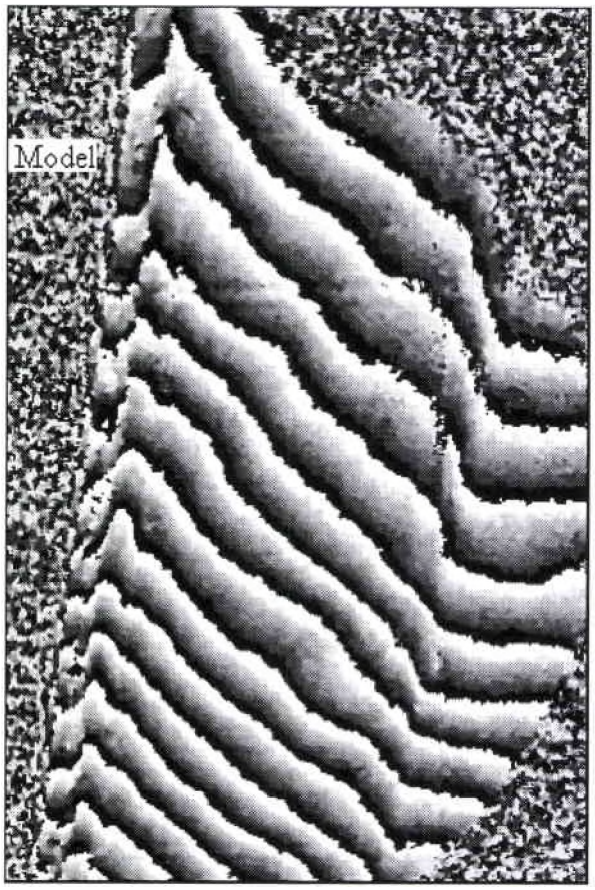

Figure 6: Phase Map of Cone at M=6

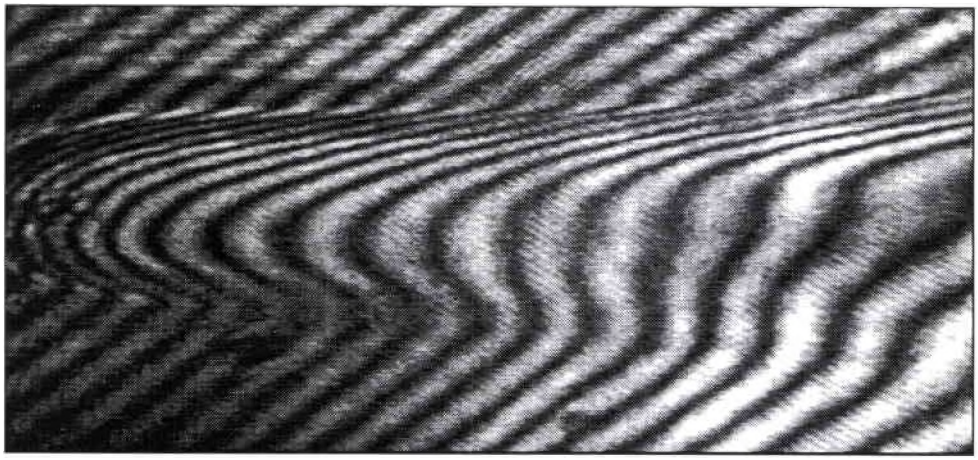

Figure 7: Interferogram of Candle

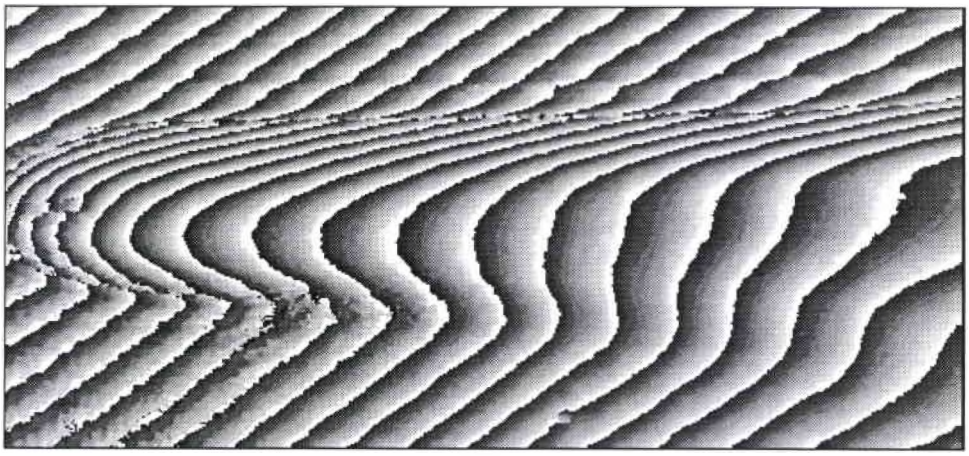

Figure 8: Phase Map of Candle Flame

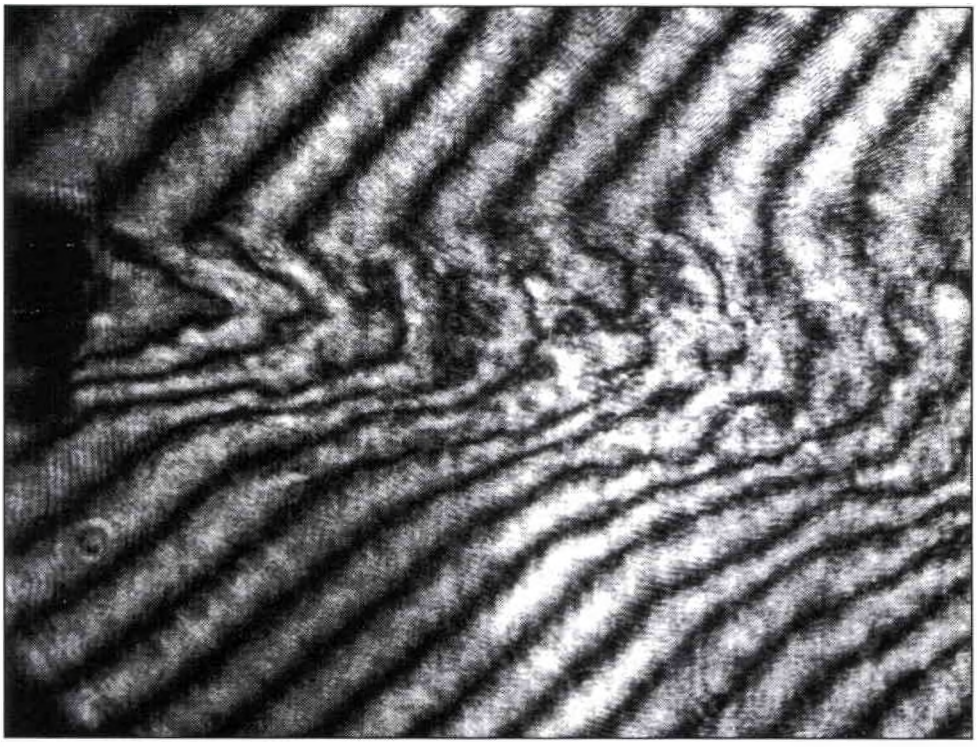

Figure 9: Interferogram of Heat Gun

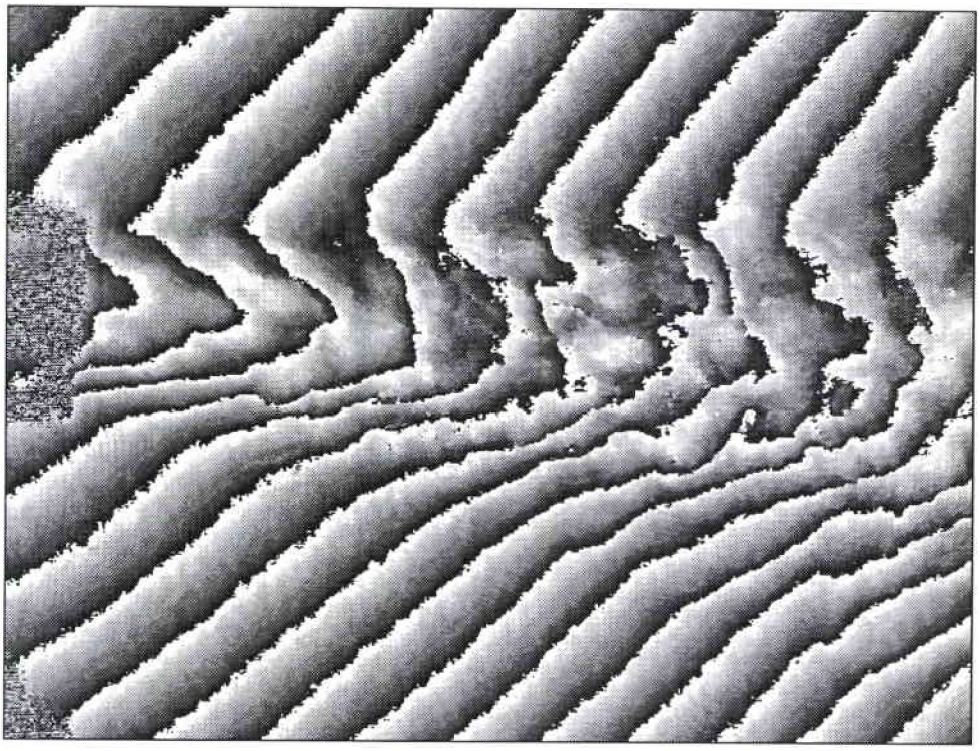

Figure 10: Phase Map of Heat Gun

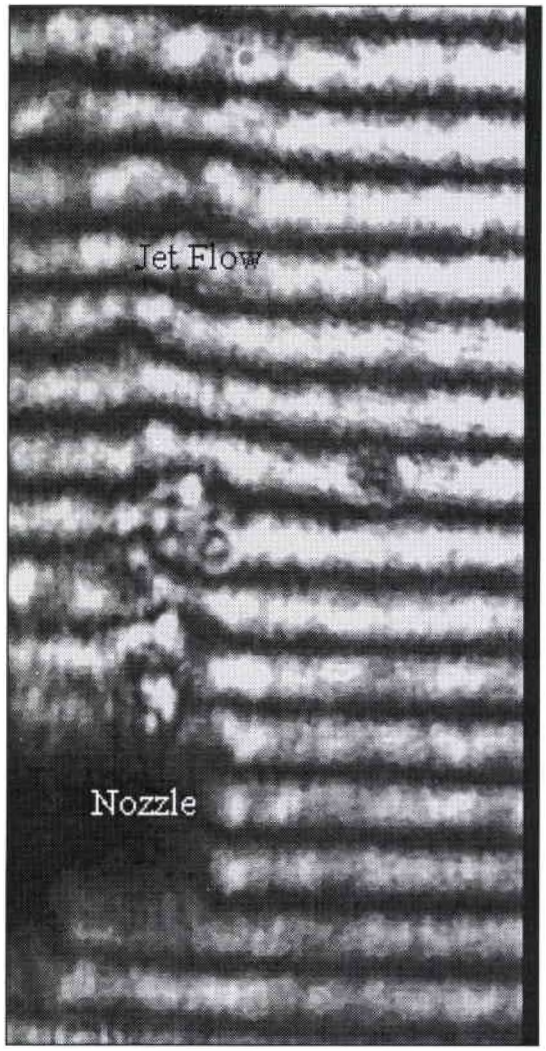

Figure 11: Interferogram of Blowing Jet P = 273.7kPa

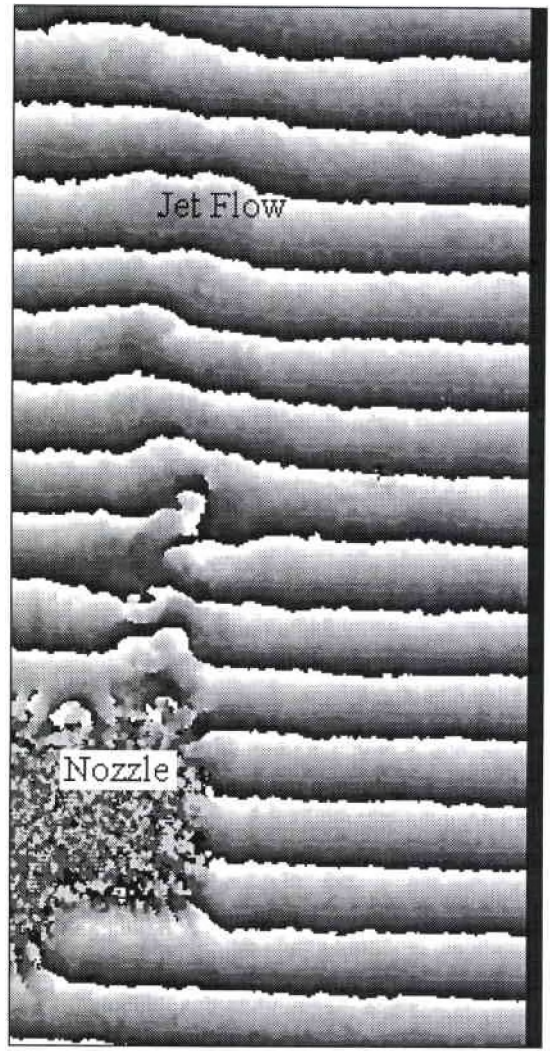

Figure 12: Phase Map of Blowing Jet P=273.6 kPa

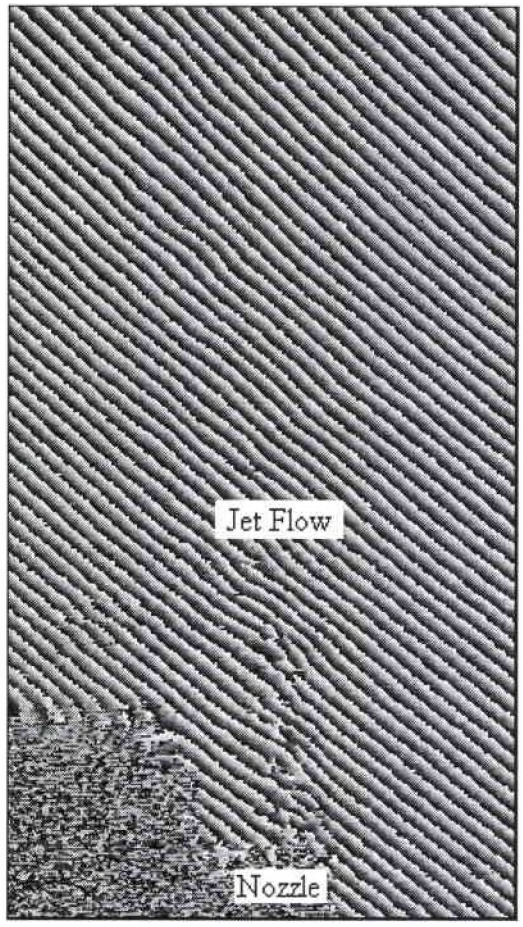

Figure 13: Phase Map of Blowing Jet P=446.1 kPa

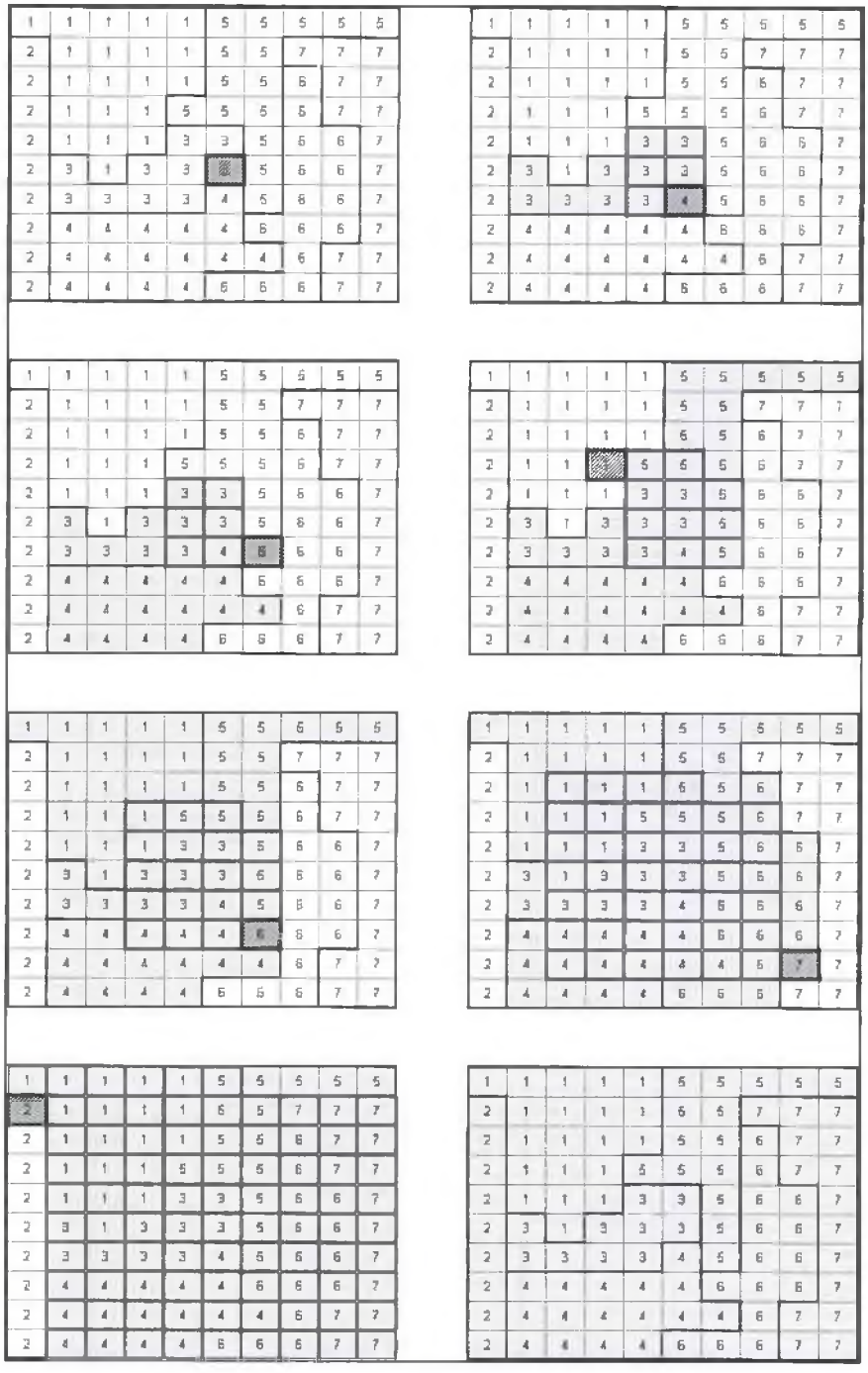

Figure 14: Example of Spiral Unwrap Method

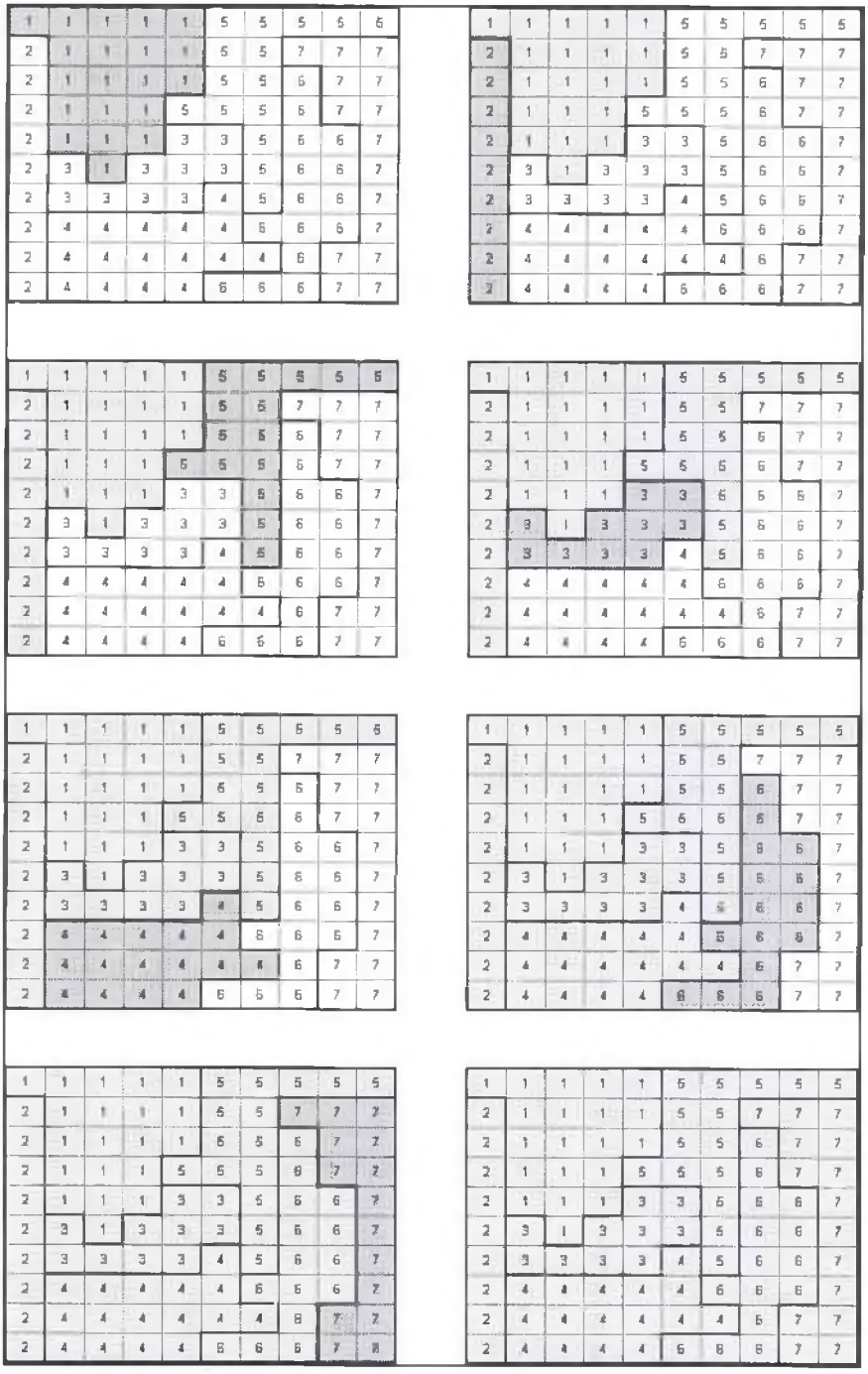

Figure 15: Example of Largest Neighbor Unwrap Method

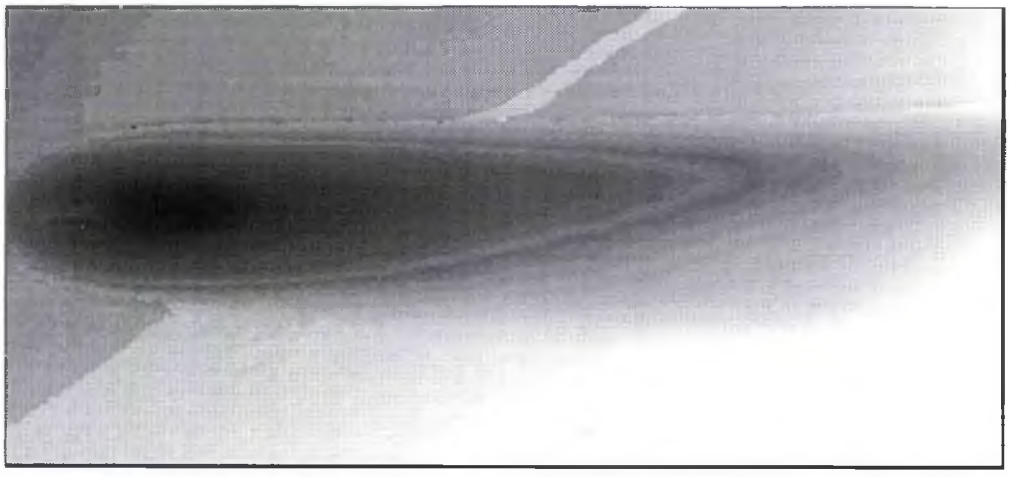

Figure 16: Unwrapped Candle uisng Spiral Method (4 Divisions)

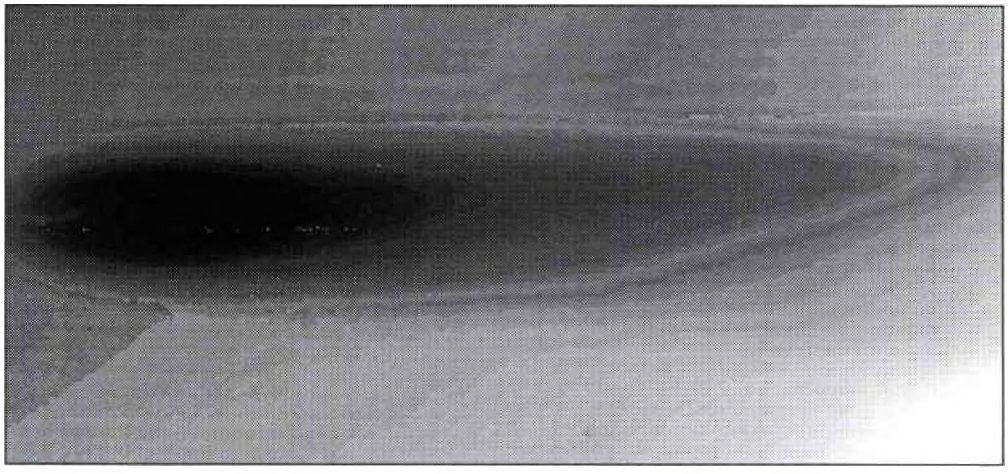

Figure 17: Unwrapped Candle using Largest Neighbor Method (4 Divisions)

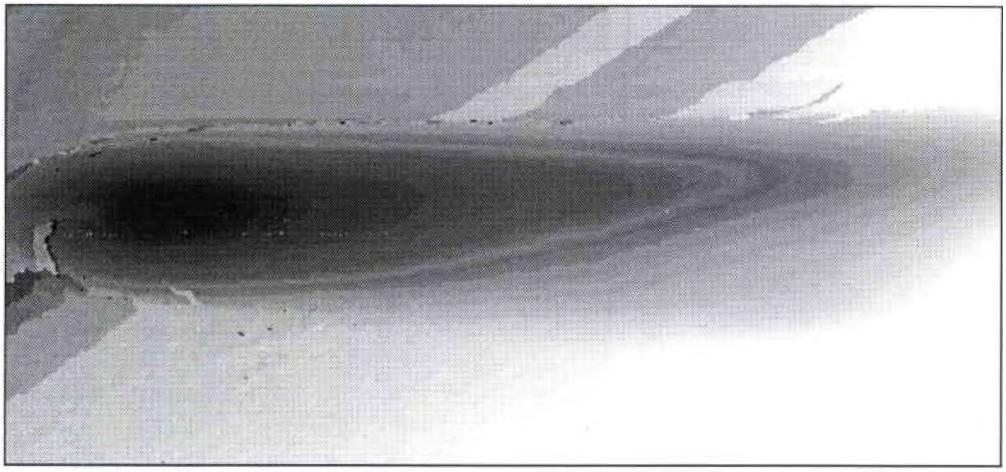

Figure 18: Unwrapped Candle using Spiral Method (8 Divisions)

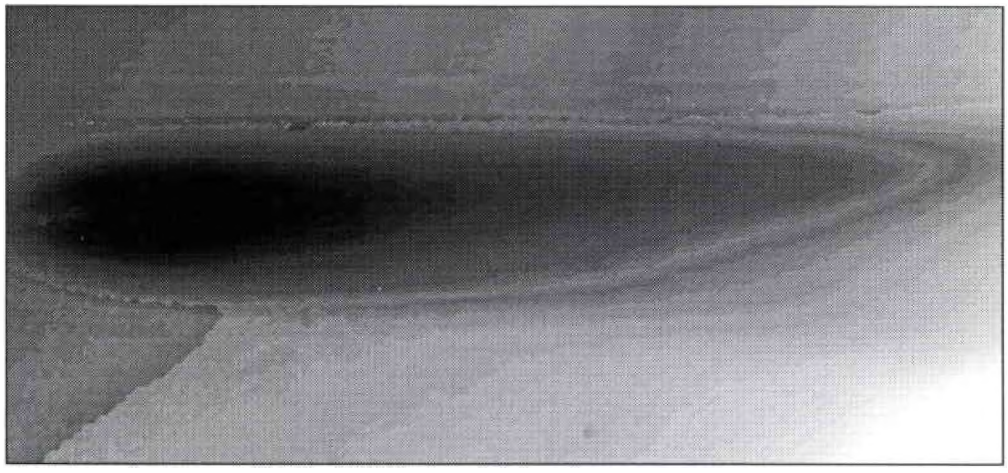

Figure 19: Unwrapped Candle using Largest Neighbor Method (8 Divisions)

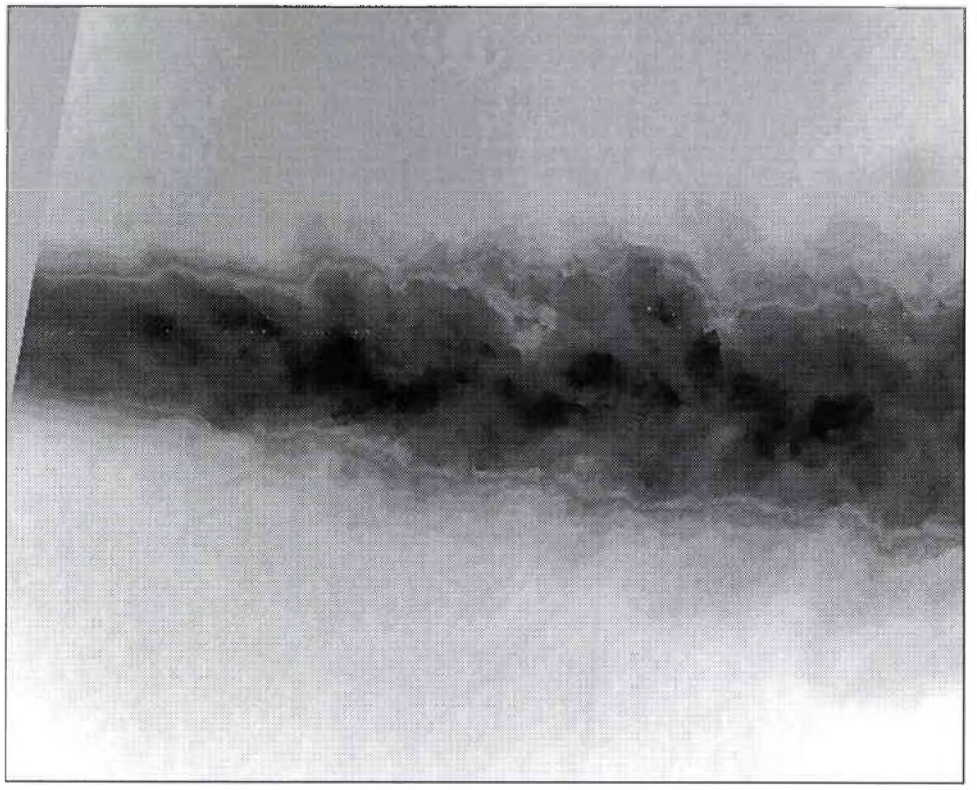

Figure 20: Unwrapped Phase Map of Heat Gun

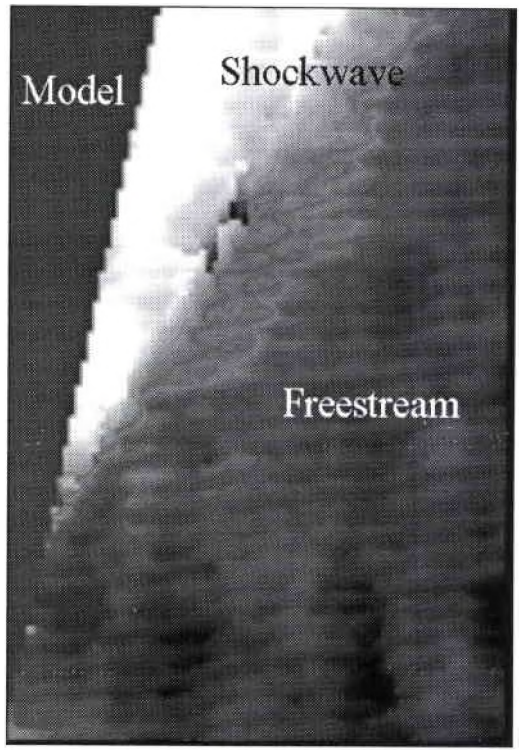

Figure 21: Unwrapped Phase Map of Wedge

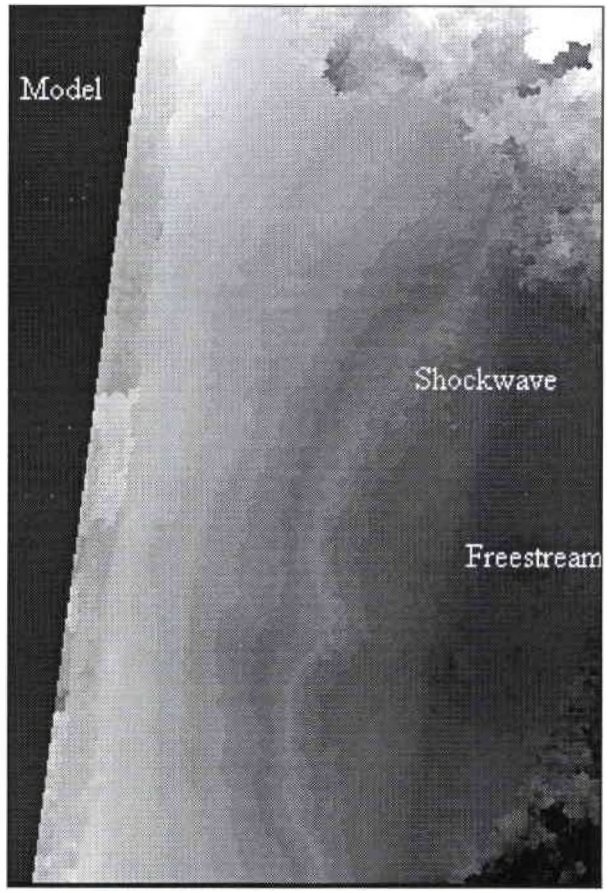

Figure 22: Unwrapped Phase Map of Cone at M=6

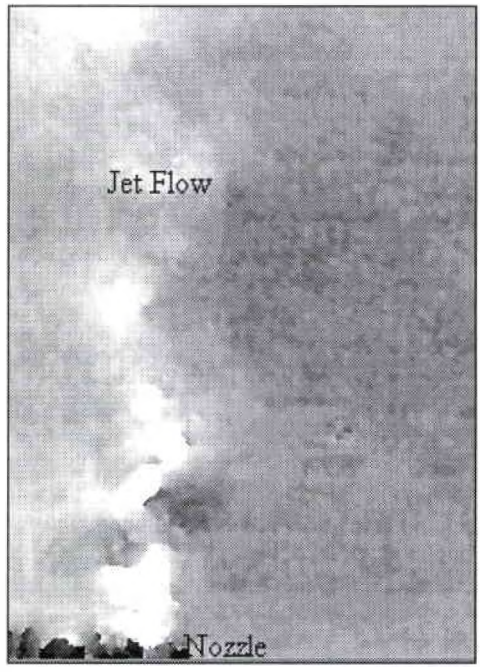

Figure 23: Unwrap of Blowing Jet P=273.7kPa

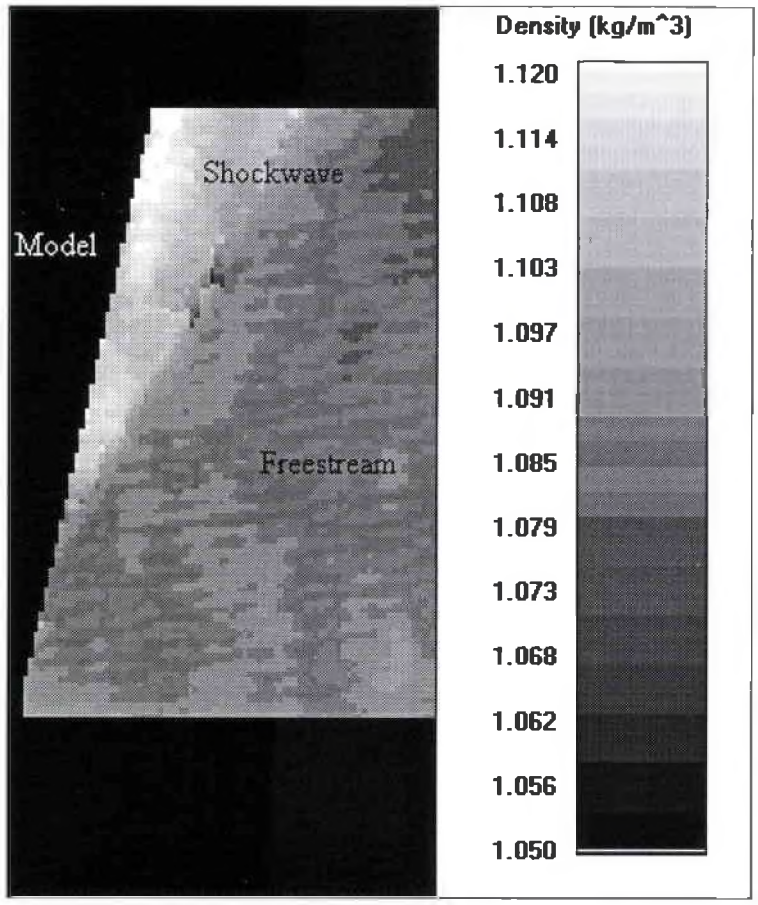

Figure 24: Density Map of Wedge Flow M=3

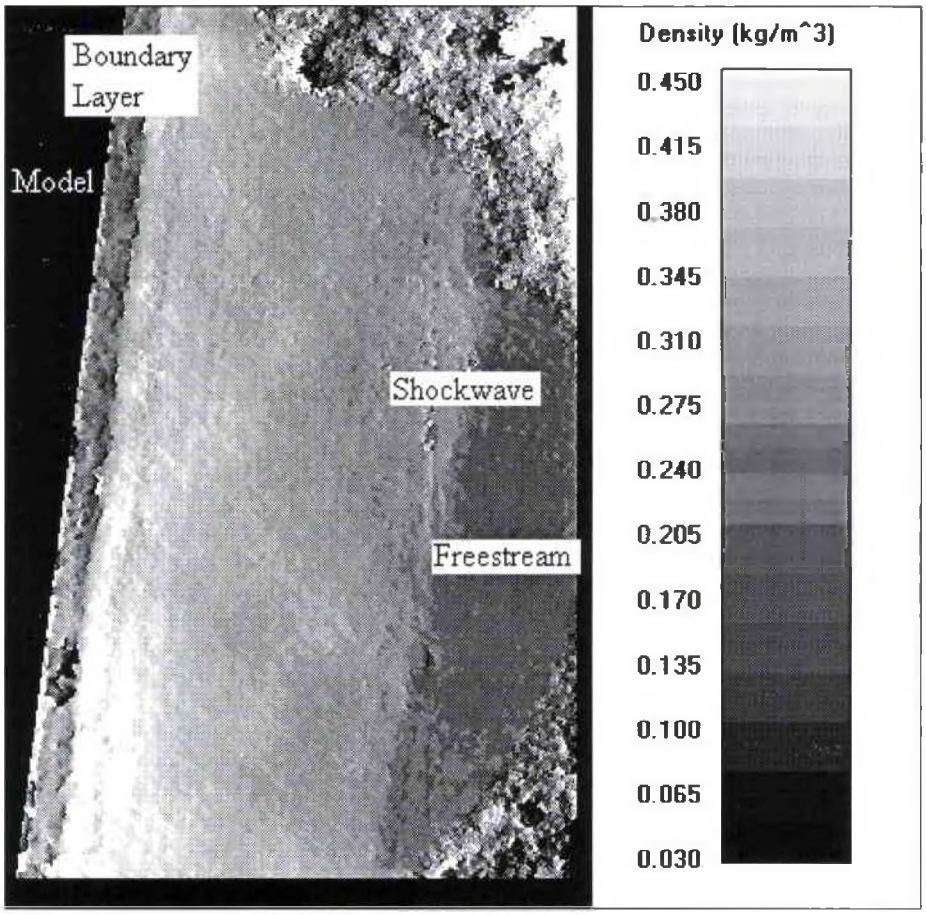

Figure 25: Density Map of Cone Flow M=6

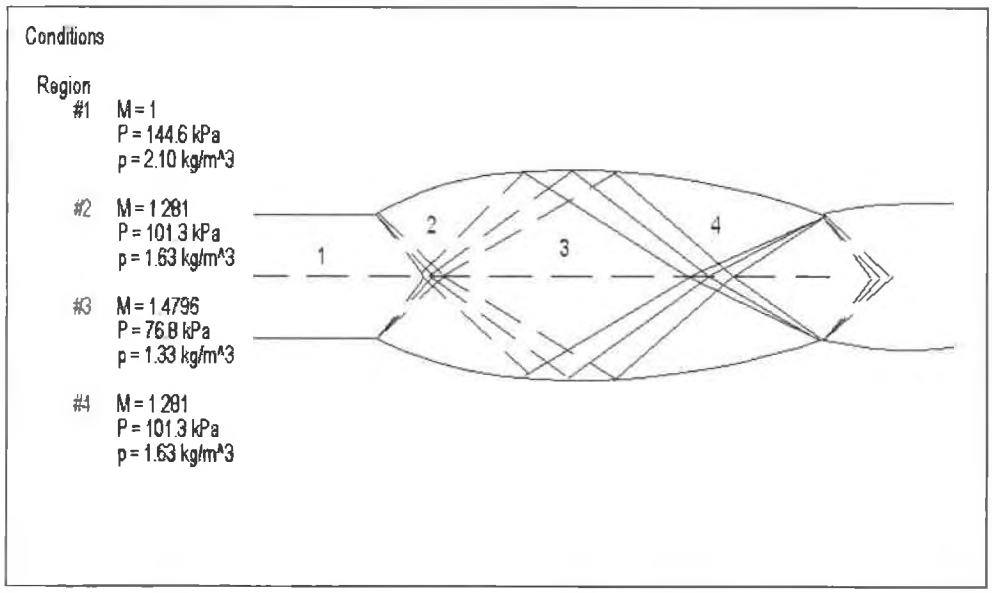

Figure 26: Analysis of Jet Flow

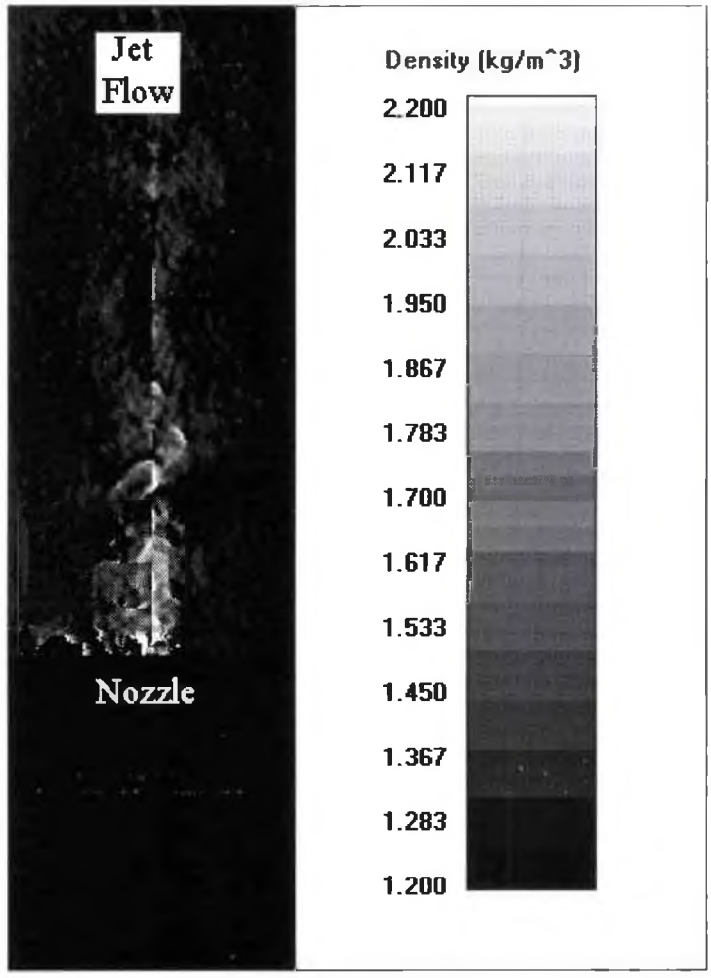

Figure 27: Density Map of Blowing Jet P=273.7kPa

VITA

Patrick Wade was born in Washington, D.C. in 1971. From 1989 to 1993, he attended Virginia Polytechnic Institute and State University as an undergraduate student in Aerospace Engineering. After receiving his B.S. he was commissioned in the US Air Force and assigned to Wright-Patterson A.F.B. as an aerospace engineer with the Experimental Diagnostics Research Section. Shortly after being stationed at Wright-Patterson, he entered the Masters program at the University of Dayton. He received his Masters in Aerospace Engineering in May 1997.

Publications/Presentations

Wade, P. and Tyler, C., "Development and Application of a Holographic Interferometry System," International Instrumentation Symposium, 43rd Meeting, May 1997, To be published.